INTERACTION NOTES

Note 226

June 1970

INTEGRAL EQUATION APPROACH TO WIDEBAND INVERSE SCATTERING:

Volume I

Development of Procedures for Numerical Solution

C. Leonard Bennett
J. D. DeLorenzo
Alethia M. Auckenthaler

Sperry Rand Research Center

ABSTRACT

The primary objective of this program was to develop practical procedures for calculating the pulse scattering characteristics of five realistic satellite shapes. Past attempts to apply frequency-domain techniques to this problem have been, at best, only partially successful. The approach taken in this program was to solve the problem directly in the time domain using a smoothed impulse function instead of a sinusoidal wave to represent the incident field. This procedure essentially eliminates the time and inaccuracy that are introduced in frequency-domain analysis by Fourier inversion of many data points, with the data at each frequency point being obtained by procedures that are comparable in complexity with our complete time-domain solution. Moreover, the time-domain solution is a relatively simple voltage versus time waveform that contains all the amplitude and phase versus frequency information over several octaves of bandwidth. By using the time domain, we have the advantage of being able to compare the computed results with those obtained on the time-domain scattering facility. This report is primarily concerned with the development of techniques to solve scattering problems involving short pulses and complicated shapes, and is presented in two volumes.

TABLE OF CONTENTS

LIST OF ILLUSTRATIONS

LIST OF ILLUSTRATIONS (cont.)

SECTION 1

INTRODUCTION

This document is submitted as the final report in response to the requirements set forth in Contract No. F30602-69-C-0332 between the Sperry Rand Research Center, Sudbury, Massachusetts and the Air Force Systems Command, Rome Air Development Center, Griffiss Air Force Base, New York. The primary objective of this program, performed during the period 12 May 1969 through 15 May 1970, was to develop practical procedures for calculating the pulse scattering characteristics of five realistic satellite shapes. Past attempts to apply frequency-domain techniques to this problem have been, at best, only partially successful.

The approach taken in this program was to recognize that since the ultimate objective is to obtain the short-pulse response, then it is more natural to solve the problem directly in the time domain using a smoothed impulse function instead of a sinusoidal wave to represent the incident field. This procedure essentially eliminates the time and inaccuracy that are introduced in frequency-domain analysis by Fourier inversion of many data points, with the data at each frequency point being obtained by procedures that are comparable in complexity with our complete time-domain solution. Moreover, the time-domain solution is a relatively simple voltage versus time waveform that contains all the amplitude and phase versus frequency information over several octaves of bandwidth.

In order to evaluate a theory the computed theoretical results should be compared with some experimentally measured results. This task would be virtually impossible from a practical standpoint if the frequency domain had been used for comparison. By using the time domain, we have the advantage of being able to compare the computed results with those obtained on the time-domain scattering facility.

This report is primarily concerned with the development of techniques to solve scattering problems involving short pulses and complicated shapes, and is presented in two volumes. The discussion of the technical approach, results and conclusions is presented in this volume (Vol. I). Computer program descriptions and listings are presented separately in Vol. II.

In Sec. 2 the general equation covering three-dimensional scattering surfaces is derived. Three procedures are developed for solution of these problems. The use of these procedures is based on the symmetries present in the problem. A problem is either asymmetric, plane symmetric or rotationally symmetric. In each of these cases numerical procedures are developed, representative calculations are made and the results are compared with those obtained experimentally.

In Sec. 3 a new integro-differential equation for obtaining the currents on a wire scatterer or antenna is developed. This equation explicitly displays the wave nature of the solution, the excitation coupling, and the loss mechanism. Procedures for numerical solution are developed and demonstrated and the results are then compared with experimental results.

The fourth section combines the procedures of Sec. 1 and Sec. 2 and results in the derivation of an integral equation that represents the currents on a three-dimensional body containing wire antennas. The procedures for solution are developed, tested on models of specific satellite shapes, and compared with measured data. The degrees of agreement in these comparisons are truly remarkable.

The final section presents a summary of the reported results and discusses the need to extend the techniques to the large-body problem.

SECTION 2

SCATTERING BY THREE-DIMENSIONAL CONDUCTING SURFACES

The general scattering problem is shown pictorially in Fig. 1. In this problem there is a magnetic field $\vec{H}^i$ incident on a conducting body which may be considered to be the field that would exist if the scatterer were not present. This incident field sets up currents $\vec{J}$ on the surface of the scatterer such that

$$\vec{J} = \hat{a}_n \times \vec{H}$$

where

$\vec{H}$ = total magnetic field

$\hat{a}_n$ = unit vector normal to surface.

These currents in turn radiate and produce the scattered magnetic field $\vec{H}^s$ which is defined as

$$\vec{H}^s \equiv \vec{H} - \vec{H}^i \quad .$$

Once the surface currents have been determined, the far field may be calculated and the scattering problem has been solved. The purpose of this section is to derive the integral equations that represent these surface currents and to develop procedures for solution of these integral equations.

2.1 DERIVATION OF THE GENERAL SPACE-TIME INTEGRAL EQUATION

One way to derive the integral equation for the surface currents is to consider the equivalent problem shown in Fig. 2, in which the scatterer has been replaced by source currents $\vec{J}$ which are equal to

$$\vec{J} = \hat{a}_n \times \vec{H} \quad .$$

Since these currents are radiating in free space, the free-space Green's

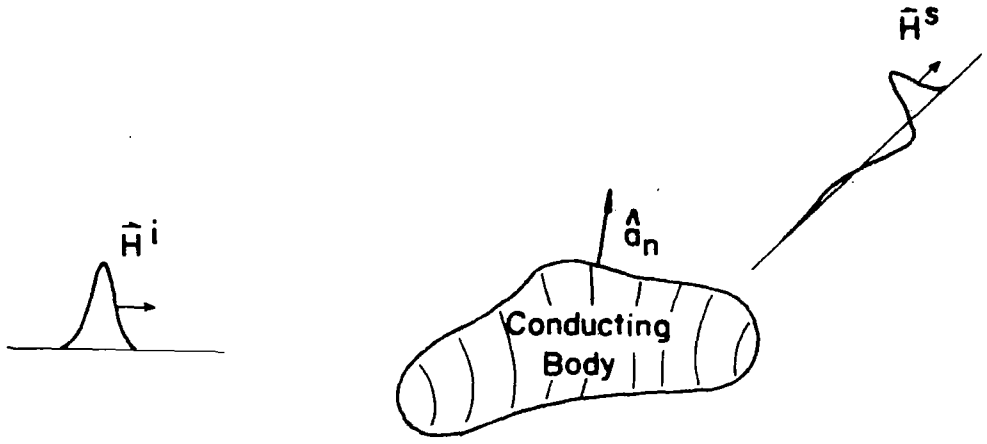

FIG. 1 General scattering problem.

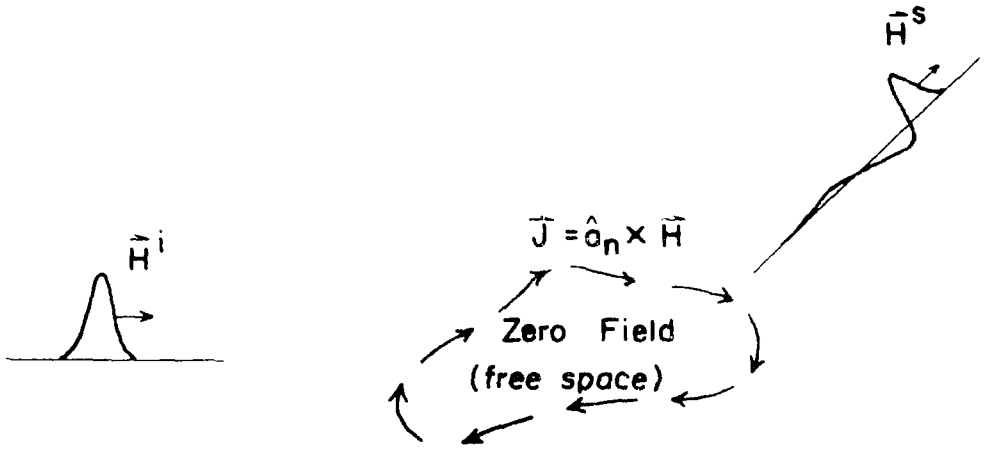

FIG. 2 Equivalent of general scattering problem.

function may be used to find the expression for the total $\vec{H}$ field at an arbitrary point in space, which is

$$\vec{H}(\vec{r},t) = \vec{H}^i(\vec{r},t) + \frac{1}{4\pi}\int_S \left\{\left[\frac{1}{R^2}+\frac{1}{Rc}\frac{\partial}{\partial\tau}\right]\vec{J}(\vec{r}',\tau)\times\hat{a}_R\right\}dS' \qquad (1)$$

$$\tau = t - R/c$$

where

$\vec{r}$ = position vector to the observation point

$\vec{r}'$ = position vector to the integration point

$R = |\vec{r} - \vec{r}'|$

$\hat{a}_R = \dfrac{\vec{r} - \vec{r}'}{R}$

c = the speed of light .

An integral equation for the current density $\vec{J}$ may be obtained by specializing the arbitrary space point $\vec{r}$ to a point on the surface of the scatterer and then applying the boundary conditions to cast $\vec{H}$ in terms of $\vec{J}$. Performing the limiting procedure and applying the boundary condition yields the integral equation

$$\vec{J}(\vec{r},t) = 2\hat{a}_n\times\vec{H}^i(\vec{r},t) + \frac{1}{2\pi}\int_S \hat{a}_n\times\left\{\left[\frac{1}{R^2}+\frac{1}{Rc}\frac{\partial}{\partial\tau}\right]\vec{J}(\vec{r}',\tau)\times\hat{a}_R\right\}dS' \qquad (2)$$

$$\tau = t - R/c$$

where $\vec{r}$ is now located on the surface of the scatterer. Equation (2) is a space-time vector integral equation for the current density $\vec{J}$ on the surface of the scatterer. The first term in the right-hand side of Eq. (2) may be considered the source term and represents the direct influence of the incident field in the current at the observation point $(\vec{r},t)$. Moreover, this term, when applied to the illuminated side of the scatterer, yields the familiar

physical-optics approximation for the surface current. The integral term on the right-hand side of Eq. (2) represents the influence of currents at other surface points on the current at $(\vec{r},t)$. The crucial observation here is that the influence of other currents on the current at $(\vec{r},t)$ is delayed by R/c , which makes numerical solution of Eq. (2) feasible.

In most applications the quantity of interest is the far scattered field. The far-field expression for the scattered magnetic field, $\vec{H}^s$, may be obtained from Eq. (1) by noting that the contribution of the first term within the integral becomes negligible when R becomes very large. In addition,

$$\hat{a}_R \rightarrow \hat{a}_r$$

and

$$\frac{1}{R} \rightarrow \frac{1}{r} \quad .$$

Thus, the expression for the far field becomes

$$\vec{H}^s(\vec{r},t) = \frac{1}{4\pi rc} \int_S \left\{ \frac{\partial \vec{J}(\vec{r}',\tau)}{\partial \tau} \right\} \times \hat{a}_r \, dS' \quad . \tag{3}$$

$$\tau = t - R/c$$

2.2 SOLUTION OF THE SPACE-TIME INTEGRAL EQUATION

The space-time integral equation in Eq. (2) represents, in principle, the complete solution of the general scattering problem for an excitation with arbitrary time dependence. However, in most practical scattering problems the incident field is a plane wave. This is the space variation which has been used to date, but it should be pointed out that the solution of the scattering problem for other space variations of the incident wave (e.g., a spherical incident wave) would be equally easy to implement. On the other hand, the time variation of the incident wave in a practical radar system can assume an arbitrary number of different forms, and although the integral equation can be used to solve each of these scattering problems separately, it is very

inefficient to do so. An efficient way to approach this problem is to compute the scattered response when the incident wave is an electromagnetic impulse. Once the electromagnetic impulse response of a particular target has been obtained, the response due to any incident wave can be calculated from it by convolving the impulse response with the specified incident waveform. Moreover, the impulse response is intimately related to the actual geometry of the target, and thus the potential for developing techniques to determine the electromagnetic impulse response of a scatterer by a simple inspection of its geometry is ever present.

For numerical solution of the space-time integral equation in Eq. (2), the incident wave was taken to be the standard Gaussian regularization of an impulse, namely,

$$\delta_n(t) = \frac{n}{\sqrt{\pi}}\, e^{-n^2 t^2} \tag{4}$$

which converges to the delta functional as n goes to infinity. The time-domain integral equation can be solved exactly for bodies with linear dimensions up to several pulse widths of this regularized impulse. In this report consideration is limited to bodies of this size.

Procedures for numerical solution of the integral equation (2) will be presented in the next sections. For this purpose, procedures are developed for three classes of scattering problems. The asymmetric scattering problem is considered in Sec. 2.3. In this case the current density must be computed and stored at all space sample points, and thus the computer time and memory are proportional to L^3, where L is the characteristic linear dimension of the scatterer. Also presented in Sec. 2.3 are procedures for solving Eq. (2) for scattering problems with symmetry about a plane. With planar symmetry present, the current density need be computed at only half the space sample points, and thus the computer time and memory are proportional to $L^3/2$. Finally, the solution of Eq. (2) for scattering problems with rotational symmetry is presented in Sec. 2.4. Since the current density need be computed at only one value of φ at each point along the axis of symmetry, the computer time for rotationally symmetric scattering problems is proportional to L. Hence, a significant saving in computer time and memory is possible if all symmetry is properly exploited.

2.3 ASYMMETRIC AND PLANE SYMMETRIC SCATTERING PROBLEMS

The space-time integral equation (2) gives the current density on the surface of an arbitrarily shaped three-dimensional scatterer due to an arbitrary incident wave. It is convenient at this point to change the units of time from seconds to light-meters, where one light-meter is defined as the time it takes an electromagnetic wave traveling at velocity c to travel a distance of one meter. This change of units facilitates interpretation of the results and removes the cumbersome factor c from the formulation and the numerical solution. Upon making this change, Eq. (2) becomes

$$\vec{J}(\vec{r},t) = 2\hat{a}_n \times \vec{H}^i(\vec{r},t) + \frac{1}{2\pi} \int_S \hat{a}_n \times \left\{ \left[\frac{1}{R^2} + \frac{1}{R} \frac{\partial}{\partial \tau} \right] \vec{J}(\vec{r}',\tau) \times \hat{a}_R \right\} dS' \qquad (5)$$

$$\tau = t - R$$

and the expression for the far scattered field, Eq. (3), becomes

$$\vec{H}^s(\vec{r},t) = \frac{1}{4\pi r} \int_S \left\{ \frac{\partial \vec{J}(\vec{r}',t)}{\partial \tau} \right\} \times \hat{a}_r \, dS' \quad . \qquad (6)$$

$$\tau = t - R$$

To handle arbitrarily shaped geometries completely, it is convenient to expand Eq. (5) in the rectangular coordinate system. Doing this gives the components of $\vec{J}$ as

$$J_x(\vec{r},t) = 2\left(n_y H_z^i - n_z H_y^i\right) + \frac{1}{2\pi} \int_S \left\{ \left(\frac{J_x}{R^2} + \frac{1}{R} \frac{\partial J_x}{\partial \tau} \right) \left(n_y n_{Ry} + n_z n_{Rz} \right) \right.$$

$$\left. - \left(\frac{J_y}{R^2} + \frac{1}{R} \frac{\partial J_y}{\partial \tau} \right) n_y n_{Rx} - \left(\frac{J_z}{R^2} + \frac{1}{R} \frac{\partial J_z}{\partial \tau} \right) n_z n_{Rx} \right\} dS' \qquad (7a)$$

$$\tau = t - R$$

$$J_y(\vec{r},t) = 2\left(n_z H_x^i - n_x H_z^i\right) + \frac{1}{2\pi}\int_S \left\{ \left(\frac{J_y}{R^2} + \frac{1}{R}\frac{\partial J_y}{\partial \tau}\right)\left(n_z n_{Rz} + n_x n_{Rx}\right) \right.$$

$$\left. - \left(\frac{J_z}{R^2} + \frac{1}{R}\frac{\partial J_z}{\partial \tau}\right) n_z n_{Ry} - \left(\frac{J_x}{R^2} + \frac{1}{R}\frac{\partial J_x}{\partial \tau}\right) n_x n_{Ry} \right\} dS' \qquad (7b)$$

$$\tau = t - R$$

$$J_z(\vec{r},t) = 2\left(n_x H_y^i - n_y H_x^i\right) + \frac{1}{2\pi}\int_S \left\{ \left(\frac{J_z}{R^2} + \frac{1}{R}\frac{\partial J_z}{\partial \tau}\right)\left(n_x n_{Rx} + n_y n_{Ry}\right) \right.$$

$$\left. - \left(\frac{J_x}{R^2} + \frac{1}{R}\frac{\partial J_x}{\partial \tau}\right) n_x n_{Rz} - \left(\frac{J_y}{R^2} + \frac{1}{R}\frac{\partial J_y}{\partial \tau}\right) n_y n_{Rz} \right\} dS' \qquad (7c)$$

$$\tau = t - R$$

where

$$\vec{J} = J_x \hat{a}_x + J_y \hat{a}_y + J_z \hat{a}_z$$

$$\hat{a}_n = n_x \hat{a}_x + n_y \hat{a}_y + n_z \hat{a}_z$$

$$\hat{a}_R = n_{Rx} \hat{a}_x + n_{Ry} \hat{a}_y + n_{Rz} \hat{a}_z \quad .$$

The coupled integro-differential equations in (7) give the solution of the current on the surface of the scatterer. However, since the current is constrained to flow on the surface, only two of these equations are independent. Hence, only two of the components of $\vec{J}$ need to be found from Eq. (7). The remaining component of $\vec{J}$ is given by

$$n_x J_x + n_y J_y + n_z J_z = 0 \qquad (8)$$

where n_x, n_y, and n_z are the rectangular components of the unit normal at the observer.

To find the far field from the current density for arbitrarily shaped geometries it is convenient to expand Eq. (6) in rectangular coordinates. Carrying out this operation yields

$$H_x^s = \frac{1}{4\pi r} \int_S \left(\frac{\partial J_y}{\partial \tau} n_{rz} - \frac{\partial J_z}{\partial \tau} n_{ry} \right) dS' \qquad (9a)$$

$$\tau = t - R$$

$$H_y^s = \frac{1}{4\pi r} \int_S \left(\frac{\partial J_z}{\partial \tau} n_{rx} - \frac{\partial J_x}{\partial \tau} n_{rz} \right) dS' \qquad (9b)$$

$$\tau = t - R$$

$$H_z^s = \frac{1}{4\pi r} \int_S \left(\frac{\partial J_x}{\partial \tau} n_{ry} - \frac{\partial J_y}{\partial \tau} n_{rx} \right) dS' \qquad (9c)$$

$$\tau = t - R$$

where

$$\vec{H}^s = H_x^s \hat{a}_x + H_y^s \hat{a}_y + H_z^s \hat{a}_z$$

$$\hat{a}_r = n_{rx} \hat{a}_x + n_{ry} \hat{a}_y + n_{rz} \hat{a}_z \quad .$$

2.3.1 Numerical Solution

The solution of the coupled set of simultaneous space-time integral equations in (7) and (8) for the surface current density was obtained by carrying out both the integration and differentiation numerically. As noted previously, only two of the components of currents need be computed using Eq. (7) and the remaining component can be obtained by applying Eq. (8). To eliminate the possibility of division by zero in Eq. (8), the current component with the largest unit normal component at a particular space sample point is the one selected to be computed with Eq. (8).

f_{xik} is the integrand of Eq. (7a) evaluated at the integration point $\vec{r}_k$ when the observer is at $\vec{r}_i$

f_{yik} is the integrand of Eq. (7b) evaluated at the integration point $\vec{r}_k$ when the observer is located at $\vec{r}_i$

ΔS_k is the surface area of the patch at $\vec{r}_k$.

The time differentiation and interpolation necessary for the evaluation of the integrands appearing in Eq. (7) were performed numerically by representing the current with a fourth-order polynomial. In order to achieve the best accuracy, the five points used for the polynomial representation of the current were chosen such that the current would be evaluated as near as possible to the middle of them. In the representation in Eq. (10) the contribution of the currents on the self patch (patch i) to the current at the observation point $\vec{r}_i$ has been neglected. Moreover, it can be shown that this contribution goes to zero as the principal radii of curvature at $\vec{r}_i$ become large. In particular, when the patch is planar, there is no contribution from the self patch. Another way of stating this condition is that the contribution from the self term is proportional to the solid angle subtended by the self patch.

It is important to note that since the minimum spacing between space sample points on the surface is greater than Δt , then Eq. (10) gives $J_x(\vec{r}_i,t)$ and $J_y(\vec{r}_j,t)$ in terms of other currents at times earlier than $(t-\Delta t)$, which are already known. Thus, Eq. (7) has been reduced from an integral equation to the recurrence formula in time given in Eq. (10) and the need to perform a matrix inversion has been eliminated.

Equation (10) is solved with a digital computer for the current density by simply marching on in time. The computation starts at a point in time before the incident field reaches the scatterer and proceeds sequentially in time in the same manner that nature would solve the problem in the real world. Once the current density has been obtained, the far scattered field is computed by performing the integration in Eq. (9) numerically.

The parameters of scatterer geometry and incident field are displayed in Fig. 3 for the asymmetric and plane symmetric scattering problems. The direction of propagation of the incident field lies in the y - z plane and makes

The surface current $\vec{J}$ is computed at points in space-time. The choice of these sample points is carried out in the following manner. First, the scattering surface is divided into curvilinear patches of approximately equal area with a space sample point at the center of each patch. The spacing of these sample points (and thus, the size of the patches) on the surface is chosen small enough to give both a good representation of the scatterer and also a good representation of the currents that exist on the scatterer. Next, the time increment Δt between the points in time at which the current is computed must be less than the time it takes a wave, moving at the speed of light, to travel between the closest space points. As will be seen later, the satisfaction of this condition insures that Eq. (7) can be solved without resorting to a matrix inversion. The first sample point in time is taken to be earlier than the time at which the incident field reaches the scatterer.

For the purpose of discussing the numerical solution of Eq. (7), it is assumed here that the x and y components of current density are computed with Eq. (7) and the z component is obtained using Eq. (8). The space integration in Eq. (7) is carried out numerically and may be represented as

$$J_x(\vec{r}_i,t) = J_x^i(\vec{r}_i,t) + \sum_{k\neq i} f_{xik}\,\Delta S_k$$

$$J_y(\vec{r}_i,t) = J_y^i(\vec{r}_i,t) + \sum_{k\neq i} f_{yik}\,\Delta S_k \qquad (10)$$

where

$\vec{r}_i$ is the position vector to the point at which the current is being computed (observation point)

$\vec{r}_k$ is the position vector to the integration point

$$J_x^i(\vec{r}_i,t) = 2(n_y H_z^i - n_z H_y^i)$$

$$J_y^i(\vec{r}_i,t) = 2(n_z H_x^i - n_x H_z^i)$$

an angle of α with the positive z axis. The polarization of the incident field is specified by the angle β , which is the angle the incident electric field vector makes with the x axis. For example, $\beta = 0$ corresponds to vertical polarization and $\beta = \pi/2$ corresponds to horizontal polarization. As indicated earlier, the scatterer surface is broken into curvilinear patches of approximately equal size. Each patch is represented by its coordinates (x_i, y_i, z_i) , its unit normal (n_{xi}, n_{yi}, n_{zi}) , and the area of the patch, ΔS_i .

A sketch of the geometry parameters used for the description of the far scattered field is drawn in Fig. 4 . In this sketch the incident field is shown propagating in the y - z plane and making an angle α with the z axis. The scattered fields produced by the surface currents are then computed in the two principal planes. The scattered field is computed in the y - z plane at angles Ψ_{yz} with respect to the direction of propagation of the incident wave. In this plane the two orthogonal components used to represent the scattered field are the component perpendicular to the y - z plane, H^s_{yzx} , and the component tangent to the y - z plane, H^s_{yzt} . The other plane in which the scattered field is computed is the p - x plane, which is formed by the direction of propagation of the incident wave and the x axis. In this plane the two components used to represent the scattered field are the component perpendicular to the p - x plane, H^s_{pxp} , and the component tangent to the p - x plane, H^s_{pxt} . These scattered fields are computed at angles Ψ_{px} which are measured with respect to the direction of propagation of the incident wave.

The procedures described above were implemented in the form of two computer programs. The computer program ASSET computes the surface currents and far fields produced by a Gaussian-shaped incident pulse for the scattering problem with no symmetry accounted for. The program description and listing of ASSET is found in Vol. II. For scattering problems with symmetry about a plane the surface currents need be computed on only one side of the plane of symmetry. For the geometry used in Fig. 3 two polarizations are treated: vertical polarization $(\beta = 0)$ and horizontal polarization $(\beta = \pi/2)$. These produce the symmetry conditions on the surface currents shown in Table I.

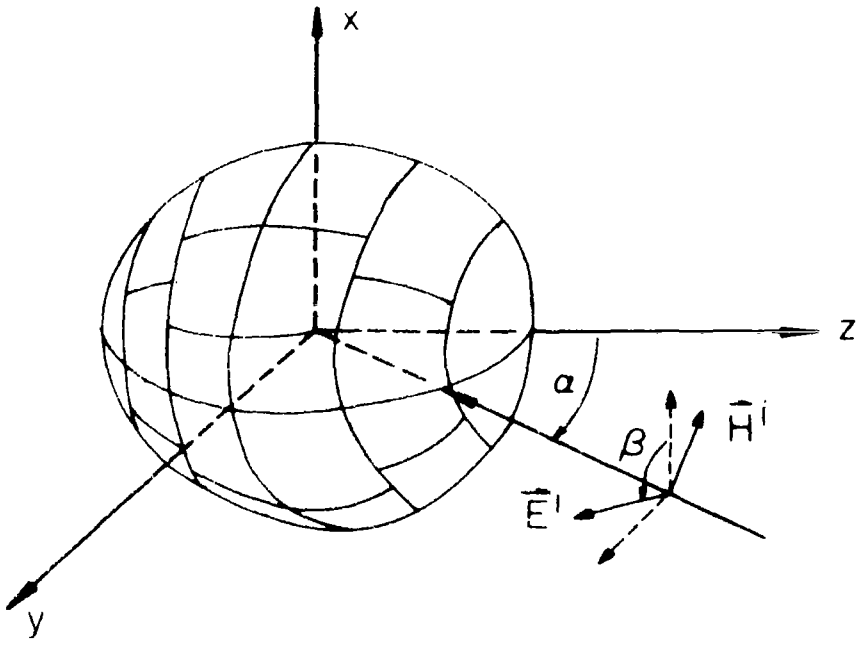

FIG. 3 Parameters of scatterer geometry and incident field for asymmetric and plane symmetric scattering problems.

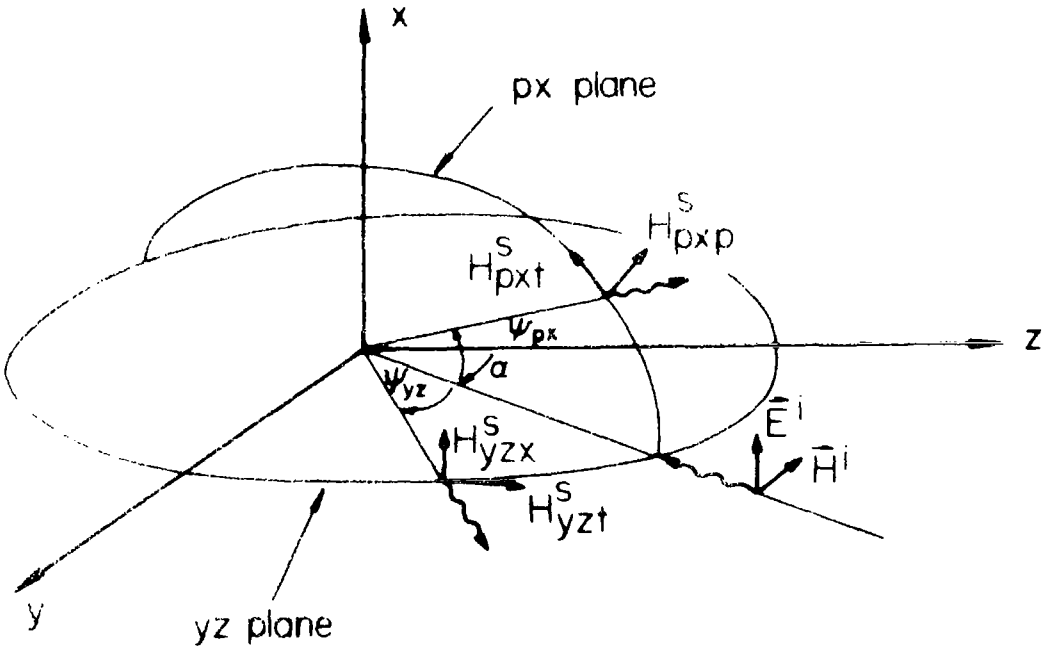

FIG. 4 Geometry parameters used for description of far scattered field.

Vertical Polarization	Horizontal Polarization
$J_x(x,y,z,t) = J_x(-x,y,z,t)$	$J_x(x,y,z,t) = -J_x(-x,y,z,t)$
$J_y(x,y,z,t) = -J_y(-x,y,z,t)$	$J_y(x,y,z,t) = J_y(-x,y,z,t)$
$J_z(x,y,z,t) = -J_z(-x,y,z,t)$	$J_z(x,y,z,t) = J_z(-x,y,z,t)$

TABLE I

Symmetry Conditions on Surface Current for Planar Symmetry

The planar symmetry conditions were incorporated and computer program PLNSY resulted. A program description and listing of PLNSY is presented in Vol. II.

2.3.2 Representative Computations

The computer program ASSET was written in response to contract requirements and solves the problem of scattering from bodies with no regard for symmetry considerations. The scatterer surface is represented by curvilinear patches and the current is computed at the center of each patch on the body. The case of a sphere with a diameter of one-half of a pulse width was used to check out the program, and for comparison with the response of the small scientific satellite model, which is presented in a later section. For this case, the sphere surface was broken into 48 patches, giving a patch size of approximately one-eighth of a pulse width on a side. The results compare well with those computed previously,[1] and the snapshot plot is displayed in Fig. 5. This figure and those that follow may be considered as space "snapshots" of the far scattered magnetic fields in which all dimensions are to scale except the distance from the scatterer. The large circle is the distance reference and represents the distance the peak of the incident pulse would have reached if it had been reflected from the origin, the center of the sphere in this case. The amplitude of the scattered field is normalized by a multiplying factor of ar_o, where a is the radius of the sphere and r_o is the distance of the far-field observer from the origin. The scattered field in the backscatter direction consists of an initial pulse, which represents the contribution due to specular

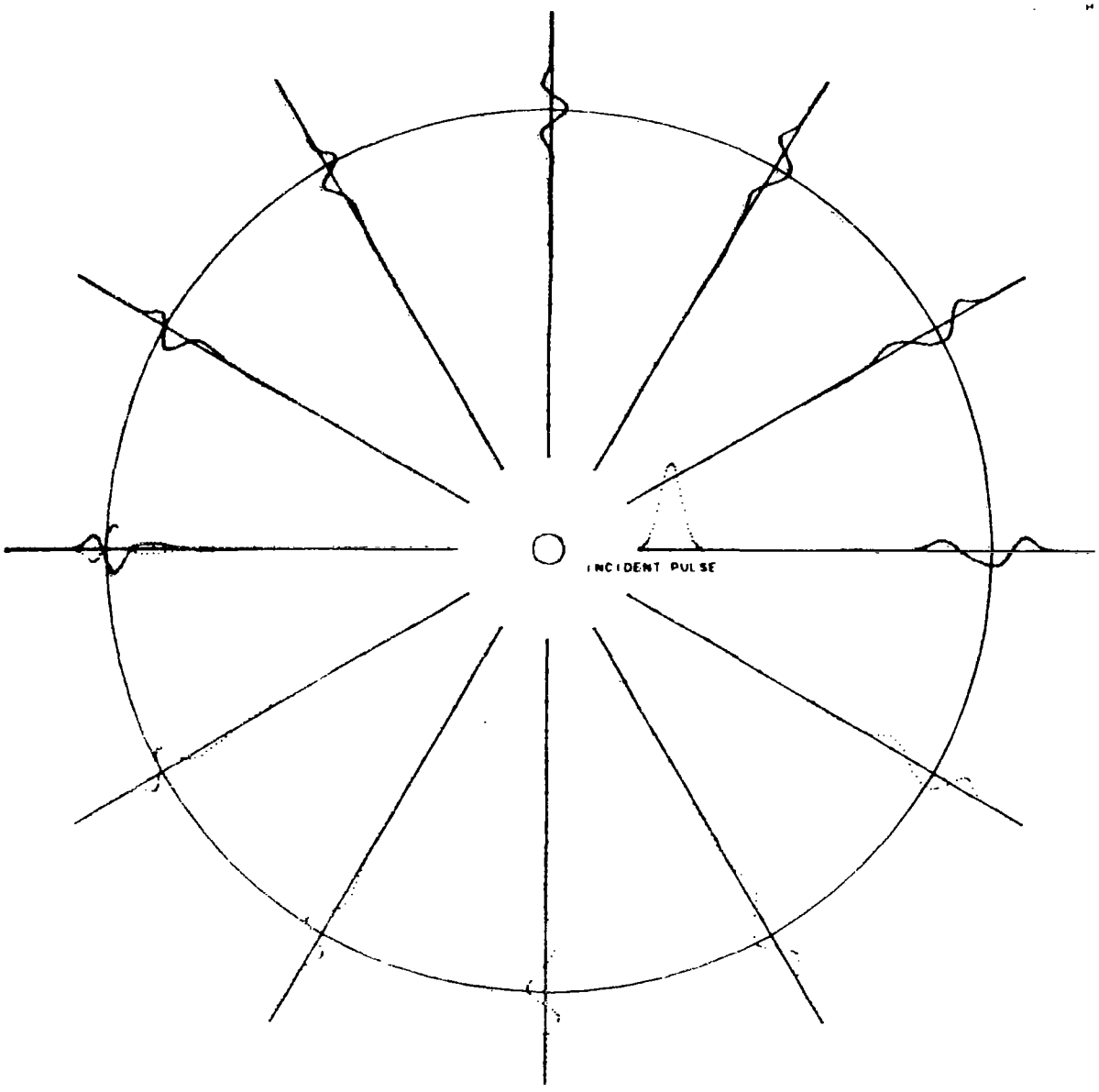

FIG. 5 Smoother impulse response of sphere computed with ASSET.

reflection, followed by a negative swing that would be predicted by the physical optics approximation. Finally, the second positive pulse may be interpreted as due to a wave traveling around the rear of the sphere. Inspection of the current density on the surface does indeed reveal two pulses, one on each side of the sphere, traveling from the illuminated side into the shadow region of the scatterer. These two current pulses continue on into the shadow region, diminishing in amplitude until they meet, at which time they coalesce and lose much of their shape and identity.

The case of scattering problems with symmetry about a plane was considered and the symmetry conditions on the surface current displayed in Table I were applied in the computer program PLNSY, which is described in Vol. II. The program was checked out initially using the case of the sphere. Some representative results of computations performed by PLNSY are displayed in Figs. 6 and 7. The smoothed impulse response of a sphere-capped cylinder with broadside incidence and with the incident electric-field vector perpendicular to the cylinder axis is shown in Fig. 6. In the backscatter direction the initial pulse is the specular return, followed by a negative swing predicted by the physical optics approximation. The second positive pulse appears at a point in time that indicates it can be attributed to a wave traveling circumferentially around the cylinder.

The smoothed impulse response in the backscatter direction from a sphere-capped cylinder with broadside incidence, but with the incident electric field polarized parallel to the cylinder axis, is shown in Fig. 7. Again, in the backscatter direction the specular return followed by a negative swing is noted. The timing of the second positive peak indicates that it is due to a wave traveling around the rear of the cylinder, but this time in the longitudinal direction. This traveling-wave mode dependence on the polarization of the incident wave was expected and has been rigorously explained by DeLorenzo.[2]

2.4 ROTATIONALLY SYMMETRIC SCATTERING PROBLEMS

In the previous section it was shown that by application of the symmetry conditions to scattering problems with planar symmetry the computer time and memory could be reduced by a factor of one-half. A further reduction in computer time can be realized in scattering problems that possess rotational

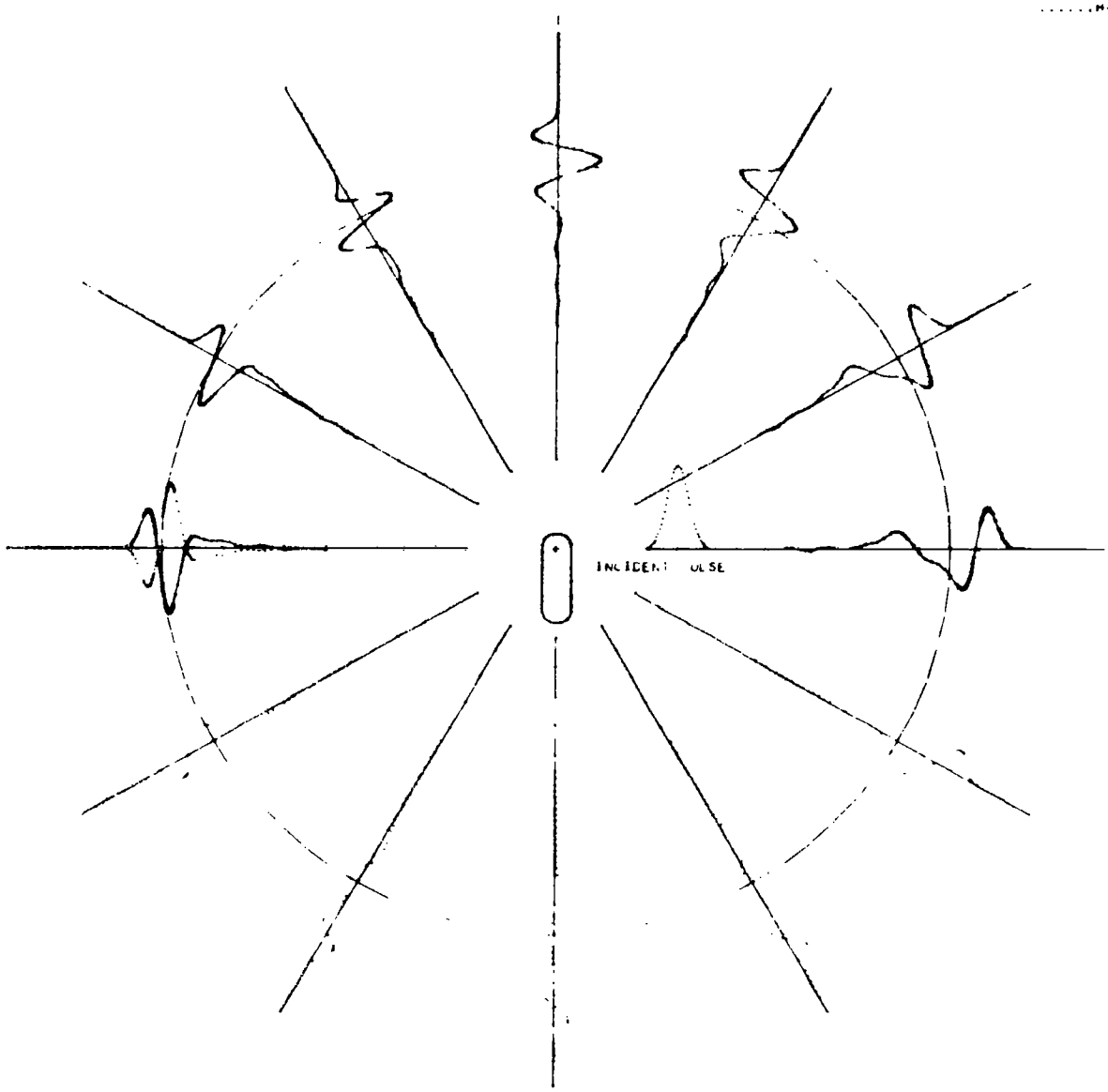

FIG. 6 Smoothed impulse response of sphere-capped cylinder (broadside incidence with perpendicular polarization).

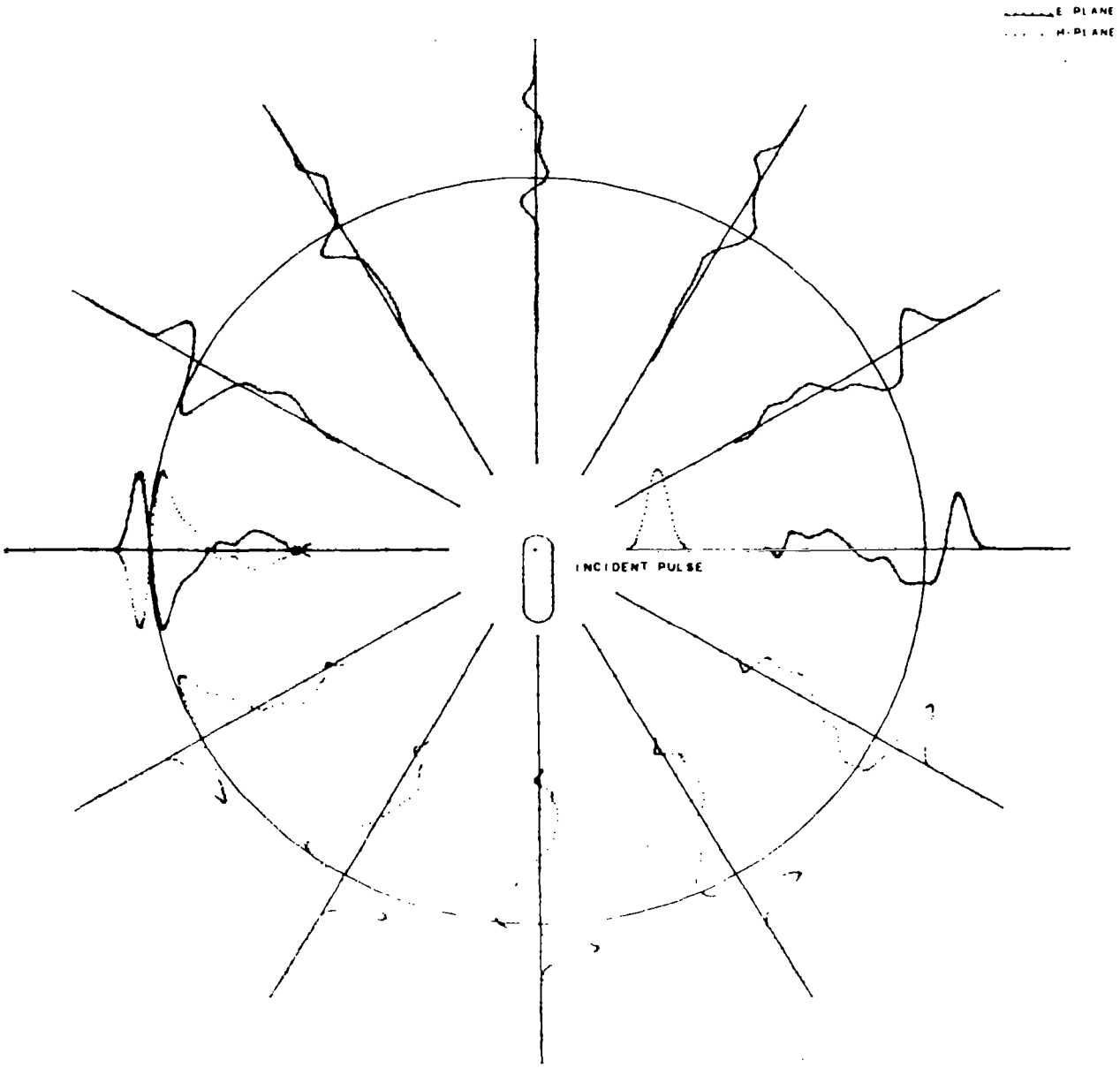

FIG. 7 Smoothed impulse response of sphere-capped cylinder (broadside incidence with parallel polarization).

symmetry, if the symmetry conditions are properly exploited. This section develops the procedures for applying the symmetry conditions to rotationally symmetric scattering problems.

The geometry of the rotationally symmetric scattering problem is displayed in Fig. 8. For convenience the polarization of the incident field was taken to be vertical, since the φ reference is arbitrary in rotationally symmetric problems. The scatterer surface is defined by the contour

$$\rho = \rho(z)$$

where ρ (the usual cylindrical coordinate) is the distance from the z axis. The contour, produced in the $y=0$ plane, starts at the most positive point in z and moves along the curve in the negative z direction. The surface is then generated by rotating the contour about the z axis. The unit vectors of interest are

$\hat{a}_n$ = the unit vector normal to the surface

$\hat{a}_2$ = the unit vector tangent to the surface which lies in the plane generated by the z axis and the position vector $\vec{r}$. (This corresponds to $\hat{a}_\theta$ in the spherical coordinate system.)

$\hat{a}_3$ = the unit vector tangent to the surface which is perpendicular to $\hat{a}_2$. (This corresponds to $\hat{a}_\varphi$ in the spherical coordinate system.)

It is also convenient to define

$$g = \frac{1}{\sqrt{1+\left(\frac{d\rho}{dz}\right)^2}} \tag{11a}$$

$$g_p = \frac{\left(\frac{d\rho}{dz}\right)}{\sqrt{1+\left(\frac{d\rho}{dz}\right)^2}} \tag{11b}$$

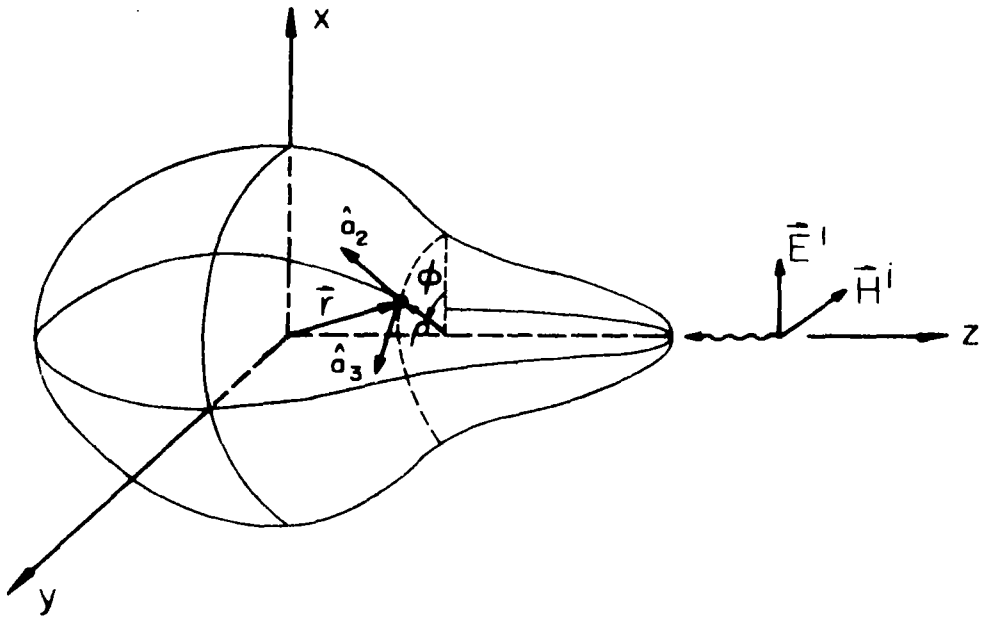

FIG. 8 Geometry of rotationally symmetric scattering problem.

which yield the following relations

$$\hat{a}_2 = - g_p \hat{a}_\rho - g \hat{a}_z \tag{12a}$$

$$\hat{a}_3 = \hat{a}_\varphi \tag{12b}$$

$$\hat{a}_n = g \hat{a}_\rho - g_p \hat{a}_z \quad . \tag{12c}$$

For reference, the space-time integral equation (5) is rewritten here:

$$\vec{J}(\vec{r},t) = 2\hat{a}_n \times \vec{H}^i(\vec{r},t) + \frac{1}{2\pi} \int_S \hat{a}_n \times \left\{ \left[\frac{1}{R^2} + \frac{1}{R} \frac{\partial}{\partial \tau} \right] \vec{J}(\vec{r}',\tau) \times \hat{a}_R \right\} dS' \tag{5}$$

$$\tau = t - R$$

Defining the source term in Eq. (5) to be

$$\vec{J}^i(\vec{r},t) = 2\hat{a}_n \times \vec{H}^i(\vec{r},t) \tag{13}$$

and carrying out the indicated cross product yields

$$\vec{J}^i(\vec{r},t) = 2H^i(z,t) \left[\hat{a}_z \cos\varphi + \hat{a}_3 g_p \sin\varphi \right] \tag{14}$$

where $\vec{H}^i(\vec{r},t)$ was taken to be

$$\vec{H}^i(\vec{r},t) = - \hat{a}_y H^i(z,t) \quad .$$

By virtue of the rotational symmetry in this problem the total surface current $\vec{J}$ may be written

$$\vec{J}(\vec{r},t) = \hat{a}_2 J_2(\ell_z,t) \cos\varphi + \hat{a}_3 J_3(\ell_z,t) \sin\varphi \tag{15}$$

where ℓ_z is the position coordinate in the $\hat{a}_2$ direction on the scatterer surface. Substituting Eqs. (14) and (15) into Eq. (5) and performing some algebra yields

$$J_2(\ell_z,t)\cos\varphi = \cos\varphi\Bigg[2H^i(z,t)$$

$$- \frac{1}{2\pi}\int_S \left[\frac{1}{R^3}+\frac{1}{R^2}\frac{\partial}{\partial\tau}\right]\Big\{J_2(\ell_z',\tau)\cos(\varphi-\varphi')$$

$$\cdot\left[\Big(g'\rho'+g_p'(z-z')\Big)\cos(\varphi-\varphi')-\rho g'\right]\Big\}\,dS'$$

$$\tau = t-R$$

$$- \frac{1}{2\pi}\int_S \left[\frac{1}{R^3}+\frac{1}{R^2}\frac{\partial}{\partial\tau}\right]\Big\{J_3(\ell_z',\tau)(z-z')\sin^2(\varphi-\varphi')\Big\}\,dS'$$

$$\tau = t-R\Bigg] \qquad (16a)$$

$$J_3(\ell_z,t)\sin\varphi = \sin\varphi\Bigg[2H^i(z,t)\,g_p$$

$$+ \frac{1}{2\pi}\int_S \left[\frac{1}{R^3}+\frac{1}{R^2}\frac{\partial}{\partial\tau}\right]\Big\{J_2(\ell_z',\tau)$$

$$\cdot\left[-g_p g'\rho'+g_p'g\rho-g_p g_p'(z-z')\right]\sin^2(\varphi-\varphi')\Big\}dS'$$

$$\tau = t-R$$

$$+ \frac{1}{2\pi}\int_S \left[\frac{1}{R^3}+\frac{1}{R^2}\frac{\partial}{\partial\tau}\right]\Big\{J_3(\ell_z',\tau)$$

$$\cdot\left[\Big(-g_p(z-z')+g\rho\Big)\cos(\varphi-\varphi')-g\rho'\right]\cos(\varphi-\varphi')\Big\}dS'\Bigg]. \qquad (16b)$$

Equations (16) are valid for any value of φ; however, it is convenient to solve Eq. (16a) for J_2 when $\varphi = 0$ and to solve Eq. (16b) for J_3

when $\varphi = \frac{\pi}{2}$. Substitution of these values of φ into Eq. (2.16) yields the following two coupled integral equations:

$$J_2(\ell_z,t) = 2H^i(z,t)$$

$$- \frac{1}{2\pi} \int_S \left[\frac{1}{R^3} + \frac{1}{R^2} \frac{\partial}{\partial \tau} \right] \left\{ J_2(\ell'_z,\tau) \cos\varphi' \right.$$

$$\left. \cdot \left[(g'\rho' + g'_p(z-z')) \cos\varphi' - \rho g' \right] \right\} dS'$$

$$\tau = t - R$$

$$- \frac{1}{2\pi} \int_S \left[\frac{1}{R^3} + \frac{1}{R^2} \frac{\partial}{\partial \tau} \right] \left\{ J_3(\ell'_z,\tau)(z-z') \sin^2\varphi' \right\} dS'$$

$$\tau = t - R \qquad (17a)$$

$$J_3(\ell_z,t) = 2H^i(z,t)\, g_p$$

$$+ \frac{1}{2\pi} \int_S \left[\frac{1}{R^3} + \frac{1}{R^2} \frac{\partial}{\partial \tau} \right] \left\{ J_2(\ell'_z,\tau) \right.$$

$$\left. \cdot \left[- g_p g'\rho' + g'_p g\rho - g_p g'_p (z-z') \right] \cos^2\varphi' \right\} dS'$$

$$\tau = t - R$$

$$+ \frac{1}{2\pi} \int_S \left[\frac{1}{R^3} + \frac{1}{R^2} \frac{\partial}{\partial \tau} \right] \left\{ J_3(\ell'_z,\tau) \right.$$

$$\left. \cdot \left[(- g_p(z-z') + g\rho) \sin\varphi' - g\rho' \right] \sin\varphi' \right\} dS' \ .$$

$$\tau = t - R \qquad (17b)$$

2.4.1 Numerical Solution

The solution of Eq. (17) is carried out on the digital computer in much the same manner as was done for the cases of asymmetric and plane symmetric problems. The surface of the scatterer is divided first into circular bands whose center is the z axis. Next, each band is divided into patches to carry out the surface integration. However, in this case, where rotational symmetry exists, it is only necessary to compute the current at the center of each band and not at the center of each patch. This produces a significant saving in computer time.

In particular, Eq. (17) is represented for numerical calculation as

$$J_2(z_i,t) = 2H^i(z_i,t)$$

$$- \frac{1}{2\pi} \sum_j \sum_\ell f_{aij\ell} \left\{ \frac{1}{R^3_{ij\ell}} + \frac{1}{R^2_{ij\ell}} \frac{\partial}{\partial \tau} \right\} J_2(z_j,\tau) \; \Delta S_\ell$$

$$\tau = t - R_{ij\ell}$$

$$- \frac{1}{2\pi} \sum_j \sum_\ell f_{bij\ell} \left\{ \frac{1}{R^3_{ij\ell}} + \frac{1}{R^2_{ij\ell}} \frac{\partial}{\partial \tau} \right\} J_3(z_j,\tau) \; \Delta S_\ell \qquad (18a)$$

$$\tau = t - R_{ij\ell}$$

$$J_3(z_i,t) = 2H^i(z_i,t) \; g_{pi}$$

$$+ \frac{1}{2\pi} \sum_j \sum_\ell f_{cij\ell} \left\{ \frac{1}{R^3_{ij\ell}} + \frac{1}{R^2_{ij\ell}} \frac{\partial}{\partial \tau} \right\} J_2(z_j,\tau) \; \Delta S_\ell$$

$$\tau = t - R_{ij\ell}$$

$$+ \frac{1}{2\pi} \sum_j \sum_\ell f_{dij\ell} \left\{ \frac{1}{R^3_{ij\ell}} + \frac{1}{R^2_{ij\ell}} \frac{\partial}{\partial \tau} \right\} J_3(z_j,\tau) \; \Delta S_\ell \qquad (18b)$$

$$\tau = t - R_{ij\ell}$$

where

z_i designates the band on which the observer is located.

z_j designates the band on which the integration point is located.

φ_ℓ designates the patch on band j on which the integration point is located.

$$f_{aij\ell} = \cos\varphi_\ell \left\{ \left[g_j \rho_j + g_{pj}(z_i - z_j) \right] \cos\varphi_\ell - \rho_i g_j \right\}$$

$$f_{bij\ell} = \sin^2\varphi_\ell \, (z_i - z_j)$$

$$f_{cij\ell} = \cos^2\varphi_\ell \left[g_{pj} g_i \rho_i - g_{pi} g_j \rho_j - g_{pi} g_{pj} (z_i - z_j) \right]$$

$$f_{dij\ell} = \sin\varphi_\ell \left\{ \left[g_i \rho_i - g_{pi}(z_i - z_j) \right] \sin\varphi_\ell - g_i \rho_j \right\}$$

$R_{ij\ell}$ is the distance between the observation point and the integration point.

The operator in the curly brackets in the integrand of Eq. (18) is represented by Lagrange's interpolation formula as

$$\left\{ \frac{1}{R^3_{ij\ell}} + \frac{1}{R^2_{ij\ell}} \frac{\partial}{\partial \tau} \right\} J(z_j, t - R_{ij\ell}) = a_{0ij\ell} \, J\left(z_j, t_{k_{ij\ell}+1} \right) + a_{1ij\ell} \, J\left(z_j, t_{k_{ij\ell}} \right)$$

$$+ a_{2ij\ell} \, J\left(z_j, t_{k_{ij\ell}-1} \right)$$

where $a_{0ij\ell}$ is the first Lagrange coefficient in a three-point representation. Moreover, some of the Lagrange coefficients in a particular band may be combined with each other because the currents for which they are coefficients are the same. Carrying out the combination and also incorporating the "f"

coefficients yields the coefficients $\underset{\sim}{a}$, $\underset{\sim}{b}$, $\underset{\sim}{c}$, and $\underset{\sim}{d}$, and Eq. (18) may be written as

$$J_2(z_i,t) = 2H^i(z_i,t) - \sum_j \sum_n^{N_{ij}} \underset{\sim}{a}_{ijn}\, J_2\left(z_j, t_{k_{ij+2-n}}\right) - \sum_j \sum_n^{N_{ij}} \underset{\sim}{b}_{ijn}\, J_3\left(z_j, t_{k_{ij+2-n}}\right) \tag{19a}$$

$$J_3(z_i,t) = 2H^i(z_i,t)\, g_{pi} + \sum_j \sum_n^{N_{ij}} \underset{\sim}{c}_{ijn}\, J_2\left(z_j, t_{k_{ij+2-n}}\right) + \sum_j \sum_n^{N_{ij}} \underset{\sim}{d}_{ijn}\, J_3\left(z_j, t_{k_{ij+2-n}}\right) \tag{19b}$$

The $\underset{\sim}{a}$, $\underset{\sim}{b}$, $\underset{\sim}{c}$, and $\underset{\sim}{d}$ coefficients in Eq. (19) represent the influence of currents at other points in space-time on the current at the observation point. These "influence" coefficients are dependent only on the geometry in the problem and not on the time dependence of the currents, and thus need be computed only once for a particular target. They may also be considered as the weighting functions for the numerical integration performed on Eq. (17). Hence, the effect of rapid variation in the geometry function of the integrands in Eq. (17) in the vicinity of edges can easily be accommodated by modifying the particular group of influence coefficients near the edge region.

Again, since the minimum spacing between space sample points is greater than Δt, then Eq. (19) gives $J_2(z_i,t)$ and $J_3(z_i,t)$ in terms of the incident field, which is known, and other currents at times earlier than $(t - \Delta\tau)$ which have already been computed. Thus, Eq. (17) has been reduced to the recurrence relation in time given in Eq. (19) and is suitable for solution on a digital computer by marching on in time.

A sketch of the geometry parameters used for the description of the far field scattered in rotationally symmetric problems is drawn in Fig. 9. In this sketch the incident field (vertically polarized) is shown propagating in the negative z direction. The scattered magnetic fields produced by the induced surface currents are then computed in the two principal planes: the E plane at angles θ_E with respect to the z axis and the H plane at angles θ_H with respect to the z axis.

Applying the rotational symmetry condition to the expression for the far scattered magnetic field given in Eq. (6) yields the scattered field in the two principal planes as

$$H_E^S(\vec{r},t_f) = \frac{1}{4\pi r}\frac{\partial}{\partial t_f}\int_S J_2(z',\tau)\cos\varphi'(g_p'\cos\varphi'\cos\theta_E - g'\sin\theta_E)\,dS'$$

$$+\int_S J_3(z',\tau)\sin^2\varphi'\cos\theta_E\,dS' \qquad (20a)$$

where

$$\tau = t_f + (\rho'\sin\theta_E\cos\varphi' + z'\cos\theta_E)$$

$t_f = t - r$ = the far-field clock

t = the surface current clock.

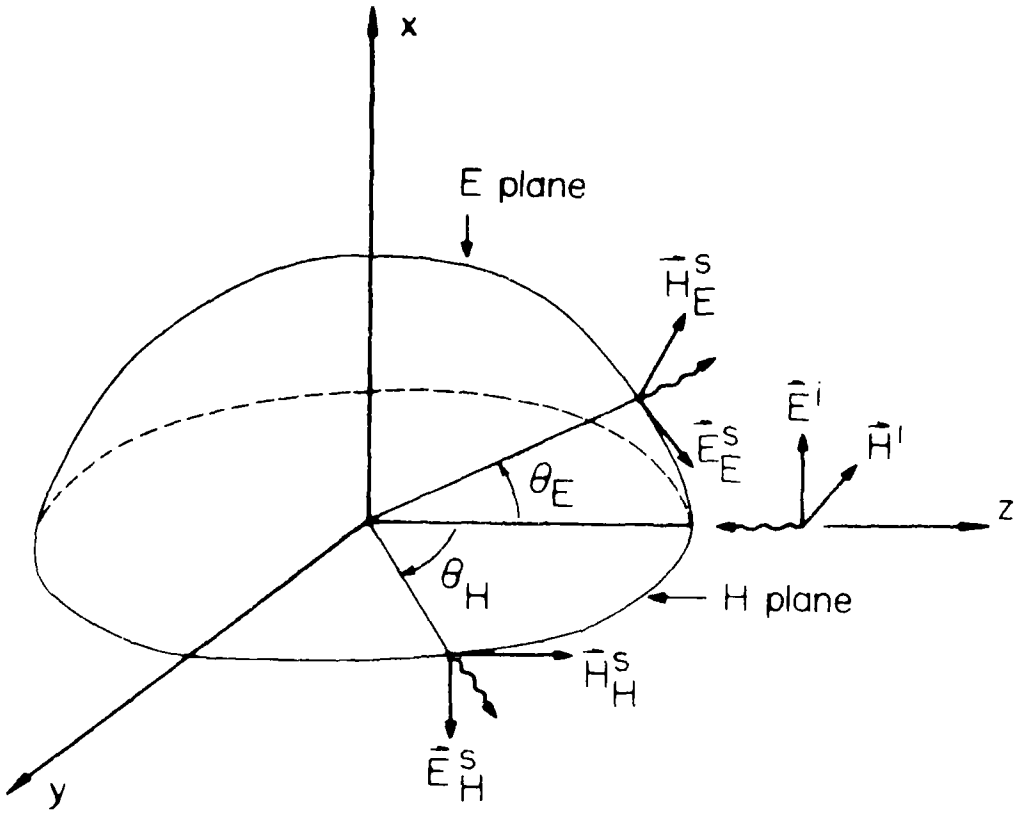

FIG. 9 Geometry parameters used for description of far scattered field in rotationally symmetric problems.

$$H_H^s(\vec{r},t_f) = \frac{1}{4\pi r}\frac{\partial}{\partial t_f}\left[\int_S J_2(z',\tau)\ g_p'\cos^2\varphi'\ dS'\right.$$

$$\left. + \int_S J_3(z',\tau)\ \sin^2\varphi'\ dS'\right] \qquad (20b)$$

where

$$\tau = t_f + (\rho'\sin\theta_H\sin\varphi' + z'\cos\theta_H)$$

The far scattered fields are computed numerically on a digital computer using Eq. (20). The integration and differentiation in these equations are performed in the same manner as was done for the asymmetric and plane symmetric problems discussed earlier.

2.4.2 Representative Computation

The computer program ROTSY was written to implement the procedures described in the previous section for the rotationally symmetric scattering problem. A program discription and listing of ROTSY can be found in Vol. II. This program was checked out initially for the case of the sphere and the results were found to be in good agreement with earlier computations without symmetry and with the inverse transform of the classical frequency-domain result. As noted earlier, the improved account of interaction in the vicinity of edges was incorporated into the influence coefficients in the neighborhood of the edge. Several smoothed impulse responses that were computed using ROTSY are now presented.

In Fig. 10 the smoothed impulse response of the advanced defense communications (ADC) satellite model is shown. As noted earlier, all dimensions are drawn to scale in this "space snapshot" except the distance from the scatterer. In the neighborhood of the origin the contour of the ADC satellite model is also shown drawn to scale. This model is a composite body made up of a right circular cylinder with a stub at one end.

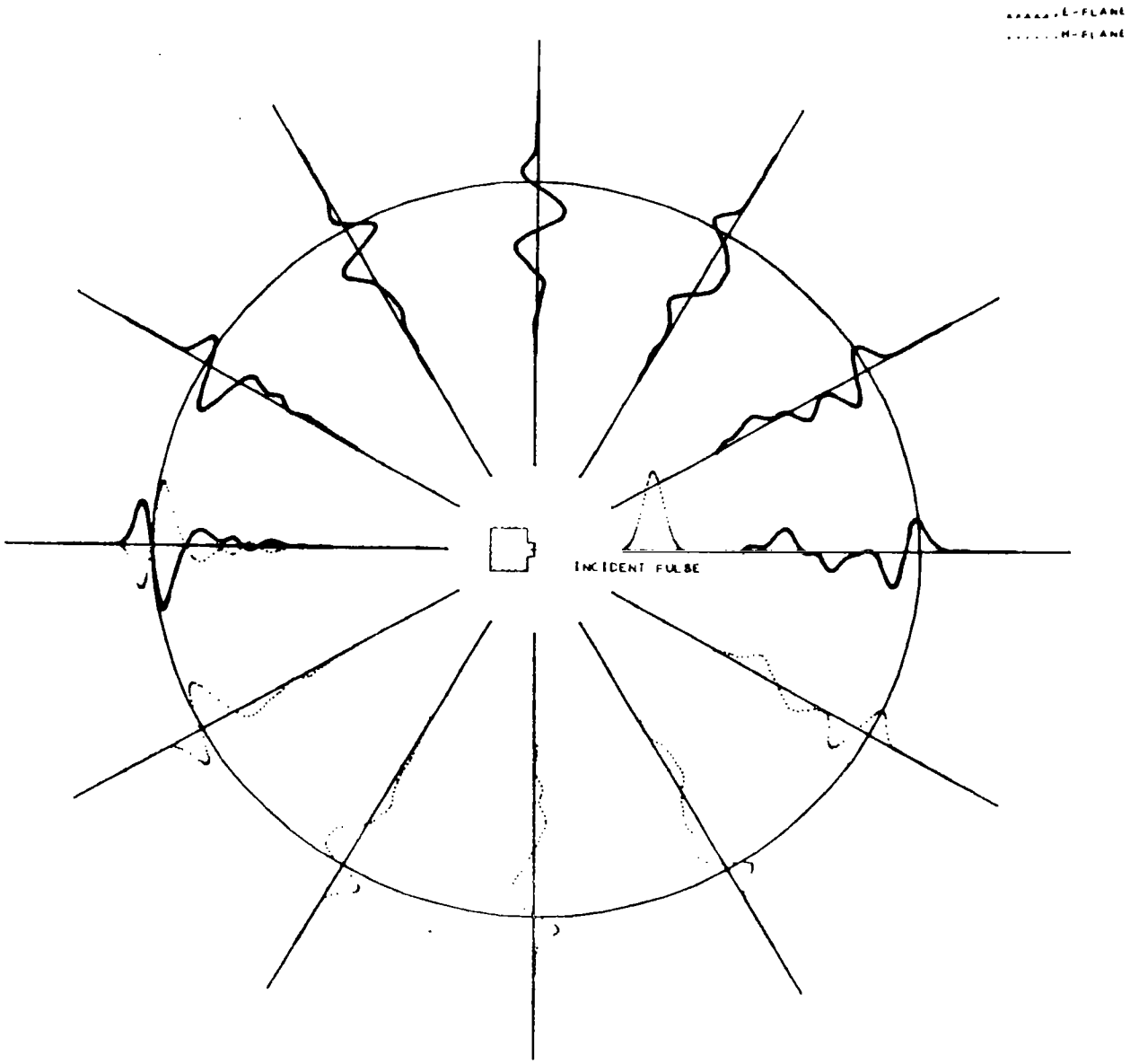

FIG. 10 Smoothed impulse response of ADC satellite model computed with ROTSY.

The space snapshot displays the scattered field in all directions. In particular, it is interesting to relate the response in the backscatter direction to the actual geometry of the target. First, the response from the stub on the target is hardly discernible. The return from the flat end of the target, however, is large and approximates the derivative of the incident pulse. This is followed by a near zero return indicating a small return in the backscatter direction from the sides of the target. Next, there is a negative pulse followed by a positive pulse. The timing of this response indicates that it can be attributed to the rear edge of the ADC satellite model.

As a check on the numerical results from ROTSY, an ADC model was fabricated and the smoothed impulse response was measured on the time-domain scattering-range facility.[3] The result is displayed in Fig. 11 and compared with the numerical calculations. The agreement is good for the return from the front end of the model and the return from the side of the model. However, the portions of the returns that may be attributed to the back edge differ from each other, with the measured result being somewhat smoother than the numerical results. This discrepancy may be due to small errors in both the numerical computation and the measured results. The numerical calculations would be improved if the band and patch size used to represent the ADC target numerically were reduced.

Figure 12 displays the smoothed impulse response of the university explorer satellite (UES) model that was computed with ROTSY. The contour of UES is shown in this figure in the neighborhood of the origin. As can be seen, this target consists of three composite right circular cylinders that may be viewed as a large right circular cylinder with a circular stub at each end. It is interesting to note that in the backscatter direction the return from the stub on the front end is clearly evident and is not completely obscured by the large return from the front end of the cylinder. This large return that follows the return from the stub again approximates the derivative of the incident pulse. However, the next region of the response is no longer near zero. Based on previous experience with the right circular cylinder and the sphere-capped cylinder the variation in this region of the response is not attributed to the sides of the large cylinder, but rather to interaction between the front stub and the front face of the cylinder. Moving further along the response, one

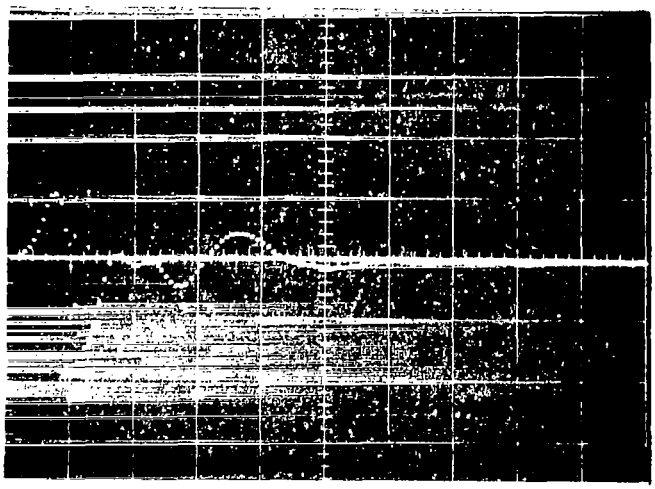

(a) Measured ADC response
(horiz. scale = 0.5 nsec/div.)

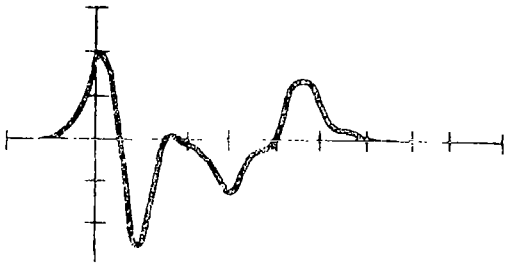

(b) Calculated ADC response

FIG. 11 Comparison of calculated and measured ADC response in backscatter direction.

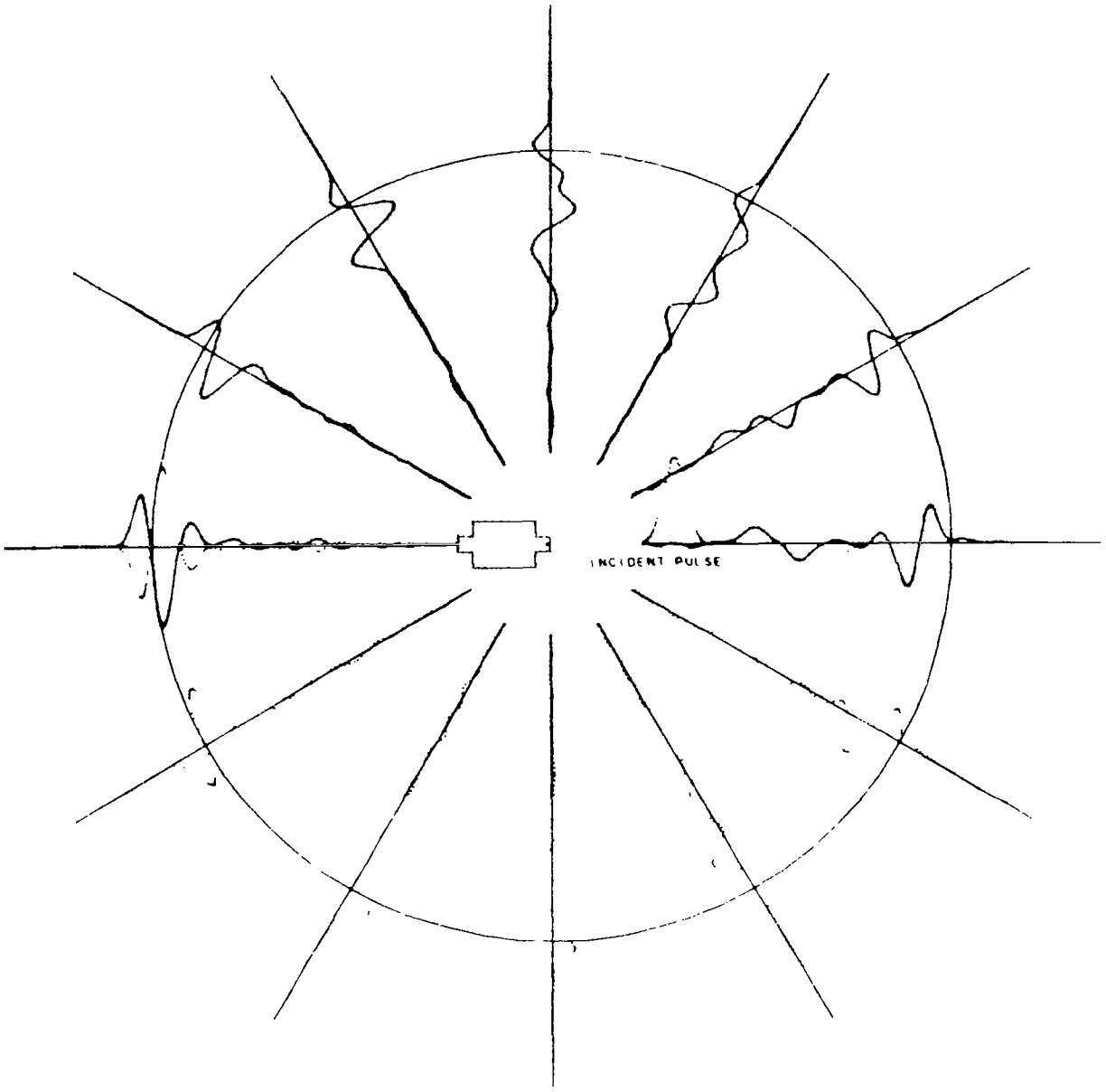

FIG. 12 Smoothed impulse response of UES satellite model computed with ROTSY.

reaches the portion that can be attributed to the return from the back edge regions of the target.

In order to check these calculated results the smoothed impulse response was measured experimentally on the time-domain scattering range. The result of this measurement is compared with the calculated result in Fig. 13. The agreement between the two results is good over the majority of the response duration.

As a final example of numerical results obtained using ROTSY, scattering from the gravity gradient test satellite No. 2 (GGTS-2) model was considered. The smoothed impulse response is displayed in Fig. 14 along with the contour of the GGTS-2 model used for the calculation. This scatterer consists of a composite of three right circular cylinders with different radii and lengths. In the backscatter direction the response from the front of the first cylinder is clearly evident and is followed by a negligible return from the sides of the first cylinder. Next, the return from the face of the second cylinder is observed, closely followed by the very large return from the face of the third cylinder. The returns from each of these faces approximate the derivative of the incident pulse, as expected. The variation in the portion of the response that appears after the return from the third cylinder face appears to be caused by interactions between the current on the third cylinder and the current on the second cylinder.

Again, the validity of the calculated results was substantiated by measuring the smoothed impulse response of a fabricated GGTS-2 model in the backscatter direction on the time-domain scattering range. The results of this measurement are in close agreement with the calculated response, as can be seen in Fig. 15.

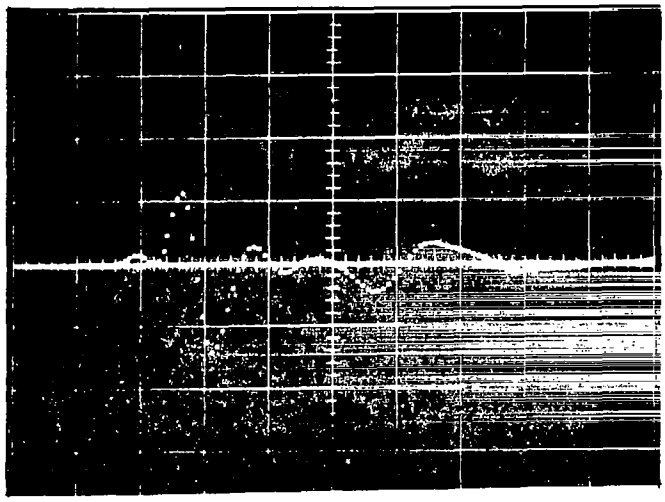

(a) Measured UES response

(horiz scale = 0.5 nsec/div.)

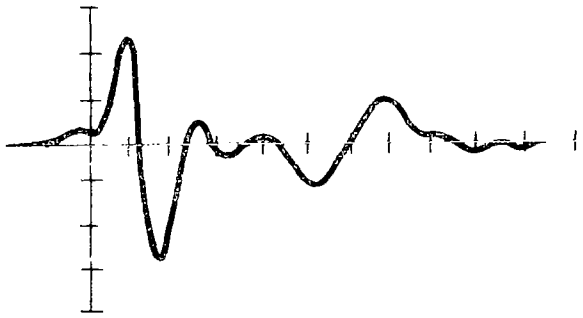

(b) Calculated UES response

FIG. 13 Comparison of calculated and measured UES response in backscatter direction.

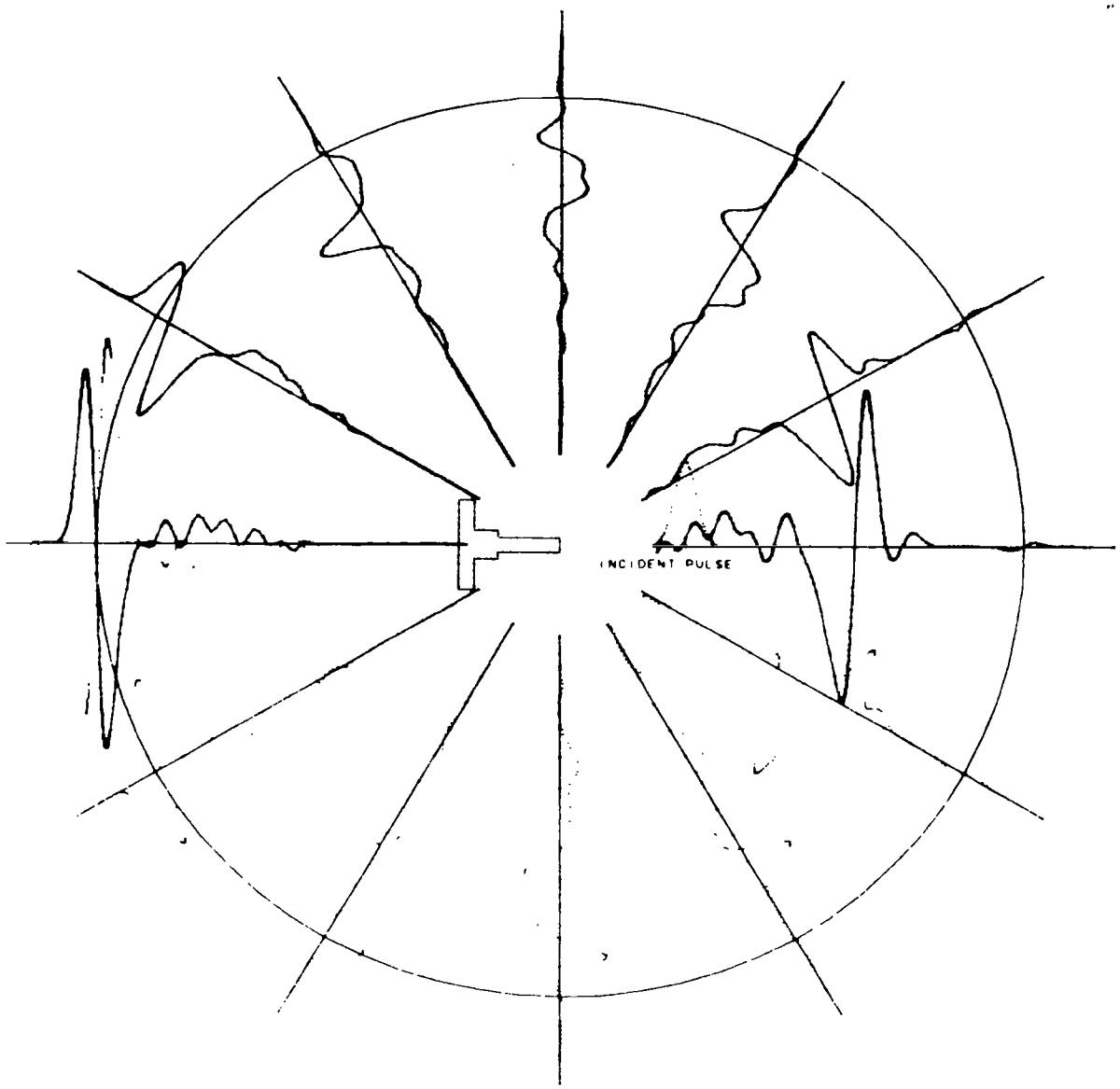

FIG. 14 Smoothed impulse response of GGTS-2 satellite model computed with ROTSY.

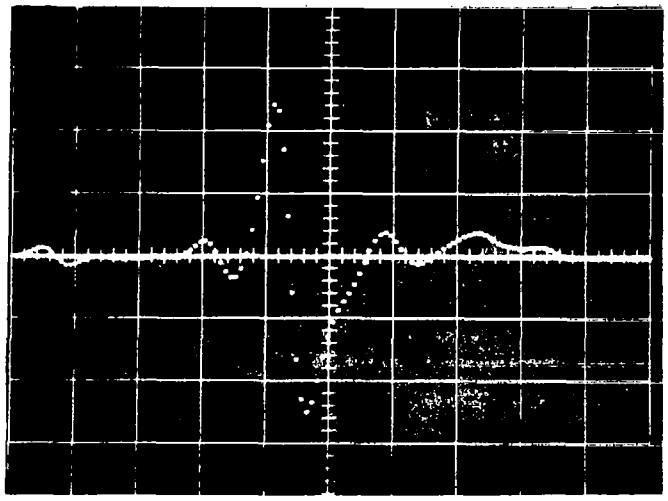

(a) Measured GGTS-2 response
(horiz. scale = 0.5 nsec / div.)

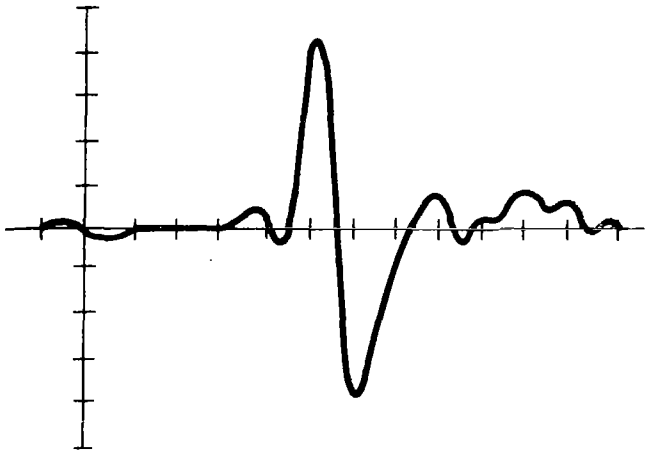

(b) Calculated GGTS-2 response

FIG. 15 Comparison of calculated and measured GGTS-2 response in backscatter direction.

SECTION 3

SCATTERING BY FINITE WIRES

The numerical solution of scattering by finite wires has been treated in some detail in the frequency domain.[4,5,6] The basic approach used in this treatment has been to make a thin-wire approximation to the electric-field integral equation and then proceed to solve the resulting integral equation numerically by matrix inversion on a high-speed digital computer. The treatment of transient scattering by finite wires in the time domain is much less well developed, and apparently the only work published to date has either been done or referenced by Sayre and Harrington.[7,8] In the technique developed by Sayre,[7] the thin-wire approximation was applied to four simultaneous field equations for the electric charge, the electric current, the electric potential, and the magnetic potential. These four equations in the time domain were then approximated numerically and solved on a digital computer. For the case of oblique angles of incidence, Sayre's results exhibited an oscillation in both the current and the far scattered-field computation that suggest chronic numerical inaccuracy in the formulation.

A different approach to the solution of the problem of transient scattering by finite wires is developed in the following sections. This approach solves the problem directly in the time domain on a digital computer by marching on in time in much the same way as was used by Sayre. However, the numerical starting point occurs after a single space-time integro-differential equation for the wire current has been formulated. In addition to eliminating analytically three of the four unknowns that Sayre eliminates numerically, this formulation provides significant insight into the transient mechanism even before numerical techniques are applied. In particular, the form into which this equation is cast specifically displays the wave character of the currents, the coupling of the currents to the excitation, and the effect of the wire ends on the currents.

3.1 DERIVATION OF SPACE-TIME INTEGRO-DIFFERENTIAL EQUATION

A straightforward way of deriving the integro-differential equation is to start with the expression for the electric field in terms of the electric

and magnetic potentials. The geometry of the problem is displayed in Fig. 17. In this particular formulation, the wire axis is parallel to the x axis and the incident wave makes an angle of θ^i with the $x=0$ plane. For this geometry, the total electric field is given by

$$\vec{E}(\vec{r},t) = \vec{E}^i(\vec{r},t) - \mu \frac{\partial \vec{A}(r,t)}{\partial t} - \nabla \vec{\varphi}(\vec{r},t) \tag{21}$$

where

$\vec{A}$ = magnetic vector potential such that $\vec{H} = \nabla \times \vec{A}$

φ = electric potential

μ = permeability of space

ϵ = permittivity of space

Next apply the Gauge relation

$$\nabla \cdot \vec{A} + \epsilon \frac{\partial \varphi}{\partial t} = 0$$

to Eq. (21) to obtain

$$\epsilon \frac{\partial \vec{E}(\vec{r},t)}{\partial t} = \epsilon \frac{\partial \vec{E}^i(r,t)}{\partial t} + \epsilon \nabla(\nabla \cdot \vec{A}) - \mu\epsilon \frac{\partial^2 \vec{A}(r,t)}{\partial t^2} \quad . \tag{22}$$

Considering only the x component and substituting the expression

$$\vec{A}(\vec{r},t) = \frac{1}{4\pi} \int_S \left\{ \frac{\vec{J}(\vec{r}',\tau)}{R} \right\} dS'$$

$$\tau = t - R/C$$

where S is the surface of the wire, into Eq. (22) yields

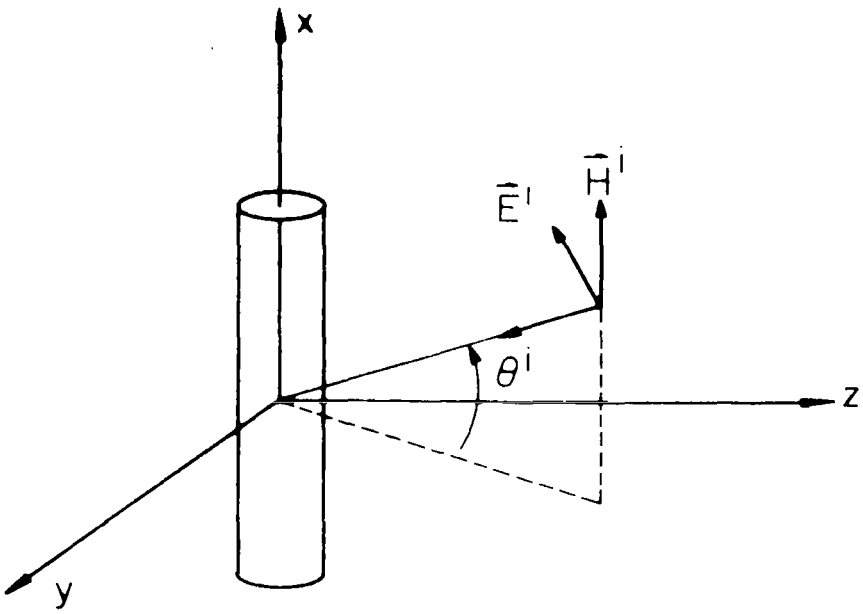

FIG. 16 Geometry of finite-wire scattering problem.

$$\epsilon \frac{\partial E_x(\vec{r},t)}{\partial t} = \epsilon \frac{\partial E_x^i(\vec{r},t)}{\partial t} + \left(\frac{\partial^2}{\partial x^2} - \frac{1}{c^2} \frac{\partial^2}{\partial t^2} \right) \left[\frac{1}{4\pi} \int_S \left\{ \frac{J_x(\vec{r}',\tau)}{R} \right\}_{\tau = t - R/c} dS' \right]. \tag{23}$$

Next, the thin-wire approximation is applied in which the width of the incident pulse is much larger than the diameter of the wire, yielding a surface current density that is independent of angular position at a particular value of x on the wire. In addition, the boundary condition on the tangential electric field at the surface of a conductor is applied to Eq. (23), yielding

$$\left(\frac{\partial^2}{\partial x^2} - \frac{1}{c^2} \frac{\partial^2}{\partial t^2} \right) \left[\frac{1}{4\pi} \int_\ell \left\{ \frac{I_x(x',\tau)}{R} \right\}_{\tau = t - R/c} dx' \right] = - \epsilon \frac{\partial E_x^i(x,t)}{\partial t} \tag{24}$$

where

ℓ = length of the wire

$R = \sqrt{a^2 + (x - x')^2}$

a = radius of wire

At this point it is convenient to change the units of time from seconds to light-meters. Carrying this out in Eq. (24) gives

$$\Box^2 \left[\frac{1}{4\pi} \int_\ell \left\{ \frac{I(x',\tau)}{R} \right\}_{\tau = t - R} dx' \right] = - \sqrt{\frac{\epsilon}{\mu}} \frac{\partial E_x^i(x,t)}{\partial t} \tag{25}$$

where

$\Box^2$ represents the wave operator $\left(\frac{\partial^2}{\partial x^2} - \frac{\partial^2}{\partial t^2} \right)$.

Finally, the wire is divided into segments and the current is evaluated at the end of each segment. For the case of the two end-points on the wire the thin-wire approximation is applied, yielding

$$I(\ell_1, t) = 0$$

$$I(\ell_2, t) = 0$$

where

$$\ell_1 = \text{lower end of wire}$$

$$\ell_2 = \text{upper end of wire} \quad .$$

For the interior points on the wire the integral over the wire that appears in Eq. (25) is evaluated over two regions: the region on which the observer is located (the self region) and the remaining region (the nonself region). The evaluation over the self region is evaluated analytically after assuming the current to be constant over it. This yields

$$\frac{1}{4\pi} \int_{\text{self}} \left\{ \frac{I(x', \tau)}{R} \right\}_{\tau = t - R} dx' = \alpha I(x, t) \tag{26}$$

where

$$\alpha = \frac{1}{2\pi} \ell n \left(\frac{\Delta x + \sqrt{\Delta x^2 + a^2}}{a} \right) \quad .$$

Substitution of Eq. (26) into Eq. (25) and rearrangement of terms gives the integro-differential equation for the current on a finite wire as

$$\Box^2 I(x, t) = -\frac{1}{\alpha} \left[\sqrt{\frac{\varepsilon}{\mu}} \frac{\partial E_x^i(x, t)}{\partial t} + \frac{1}{4\pi} \Box^2 \int_{\text{nonself}} \left\{ \frac{I(x', \tau)}{R} \right\}_{\tau = t - R} dx' \right] \tag{27}$$

It is interesting to note that this integro-differential equation displays the wave character of the currents by virtue of the wave operator on

the left-hand side. Moreover, it also displays the coupling between the excitation $E_x^i(r,t)$ and the current through the coefficient α. Finally, the effect of the ends of a nonzero radius wire on the current is contained in the second term on the right-hand side of Eq. (27).

The expression for the far scattered field for the case of finite wires can be obtained by applying the thin-wire approximation to Eq. (6), which yields

$$H^S(\vec{r},t_f) = \frac{1}{4\pi r}\int_{\ell}\left\{\frac{\partial I(x',\tau)}{\partial t}\right\}\, dx' \quad \sin\theta_E \tag{28}$$

where

θ_E is defined in Fig. 9

$\tau = t_f + x' \cos\theta_E$

$t_f = t - r$ = the far field clock

t = the wire current clock.

3.2 NUMERICAL SOLUTION

The numerical solution of Eq. (27) was accomplished by treating the right-hand side as a forcing function that is known. This is possible in this case since the right-hand side contains only the incident field, which is known, and wire currents that have been previously computed. Thus, the problem is then reduced to the solution of a one-dimensional wave equation with a forcing function. This was accomplished numerically on a digital computer by marching on in time using the standard five-point difference approximation to the one-dimensional wave operator.[9]

In this solution the wire was divided into equal-length segments and the current was computed at the end of each segment. The time increment Δt was chosen less than or equal to the length of the space segments to insure stability of the solution.[9] This choice also insures that the right-hand side of Eq. (27) is a function of entirely known quantities.

Using a five-point difference approximation of the wave operator, Eq. (27) may be represented numerically as

$$\left(\frac{I_{i-1,j-1} - 2I_{i,j-1} + I_{i+1,j-1}}{\Delta x^2} - \frac{I_{i,j-2} - 2I_{i,j-1} + I_{i,j}}{\Delta t^2} \right) = -F_{i,j-1} \qquad (29)$$

where

$$I_{i,j} = I(x_i, t_j)$$

Δx = space increment

Δt = time increment

$$F_{i,j} = \frac{1}{\alpha} \left[\sqrt{\frac{\epsilon}{\mu}} \frac{\partial E_x^i(x_i, t_i)}{\partial t} + \frac{1}{4\pi} \Box^2 g_{ij} \right]$$

$$g_{ij} = \int_{\ell_1}^{x_{i-1}} \left\{ \frac{I(x', \tau)}{R} \right\}_{\tau = t_j - R} dx' + \int_{x_{i+1}}^{\ell_2} \left\{ \frac{I(x', \tau)}{R} \right\}_{\tau = t_j - R} dx' \quad .$$

The integration in g_{ij} was performed numerically by using the trapezoidal rule and the wave operator was applied to g_{ij} by means of the five-point difference approximation. The recurrence relation for the current on a finite wire may be obtained by rearranging terms in Eq. (29) and becomes

$$I_{i,j} = \Delta t^2 F_{i,j-1} + \frac{\Delta t^2}{\Delta x^2} \left(I_{i-1,j-1} - 2I_{i,j-1} + I_{i+1,j-1} \right) - \left(I_{i,j-2} - 2I_{i,j-1} \right) \qquad (30)$$

Equation (30) is solved on a digital computer for the current density by simply marching on in time. This computation starts at a point in time

before the incident field reaches the wire and proceeds sequentially in the same manner as was used for the solution of the space-time integral equation for surface scatterers. Once the wire current has been obtained, the far scattered field is computed on a digital computer using a numerical representation of Eq. (28).

3.3 REPRESENTATIVE COMPUTATIONS

The computer program WSCAT was written to implement the procedures described in the previous section for the solution of the transient finite-wire scattering problem. A program description and listing of WSCAT is included in Vol. II. This program was initially checked out for the infinite-wire case and the result was in good agreement with the inverse transform of the classical frequency response. In addition, the far fields scattered by wires of various length-to-diameter ratios were measured on the time-domain scattering range[3] and compared with the results calculated with WSCAT. An example of the good agreement obtained is shown in Fig. 17 for the case of a finite wire with a length-to-diameter ratio of 10 and a diameter of one-tenth of a pulse width. The wave shape, the period, and the rate of damping are in close agreement in the two results.

In Fig. 18 the space snapshot of the response from a finite wire with a length-to-diameter ratio of 10 and normal incidence is shown. Note that the response has decayed to less than one-tenth of the first peak value after three periods of the response and that the distance between zero crossings is approximately 1.25 times the time it takes a wave moving at the velocity of light to traverse the length of the wire.

The smoothed impulse response of a thinner wire ($L/D = 100$) with normal incidence is shown in Fig. 19. Note that for this thinner wire the response is smaller but decays more slowly than for the case of the wire in Fig. 18. In addition, the distance between zero crossings is reduced to approximately 1.08, as expected. In the limit of zero wire thickness the distance between zero crossings approaches the time it takes a wave to traverse the length of the wire traveling at the speed of light; however, the amplitude of the response will approach zero. This effect is predicted by the integro-differential Eq. (27) since α goes to infinity as the wire radius goes to zero.

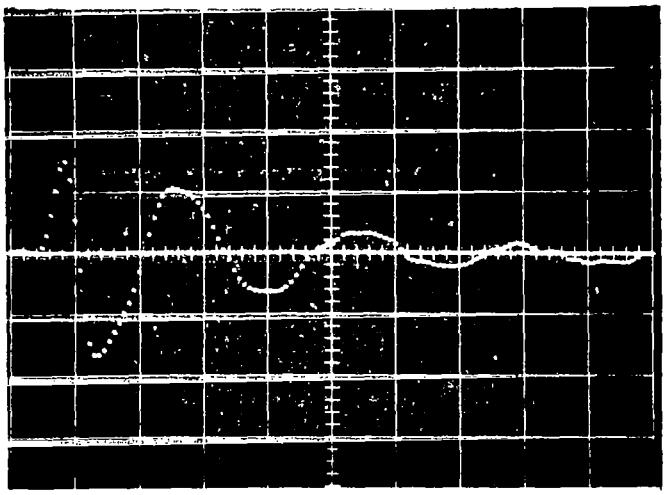

(a) Measured finite wire response (L/D = 10)
(horiz. scale = 0.5 nsec/div.)

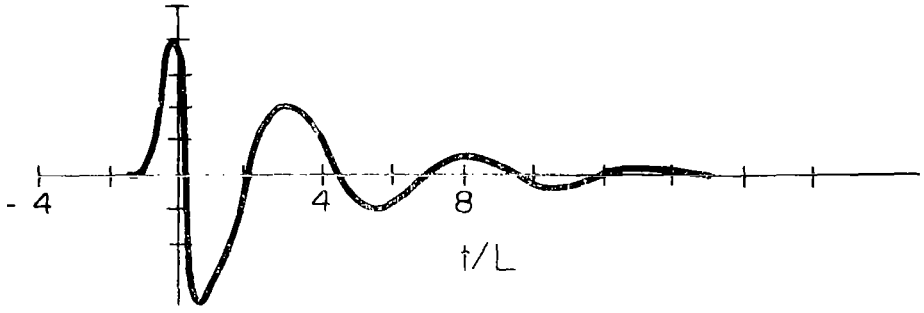

(b) Calculated finite wire response (L/D = 10)

FIG. 17 Comparison of calculated and measured finite-wire response in backscatter direction.

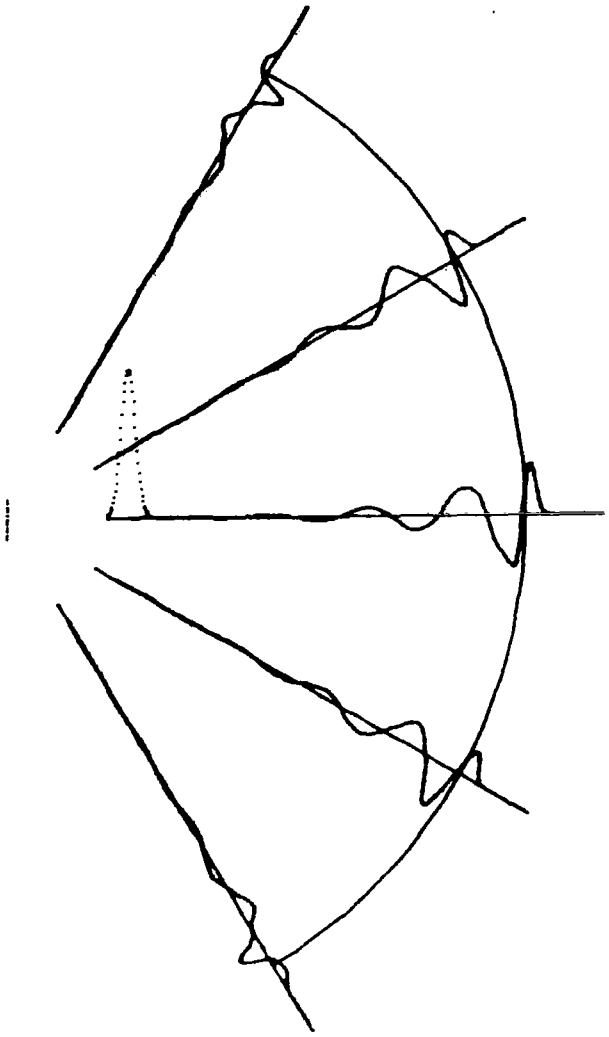

FIG. 18 Smoothed impulse response of finite wire with L/D=10 and θ^i 0°.

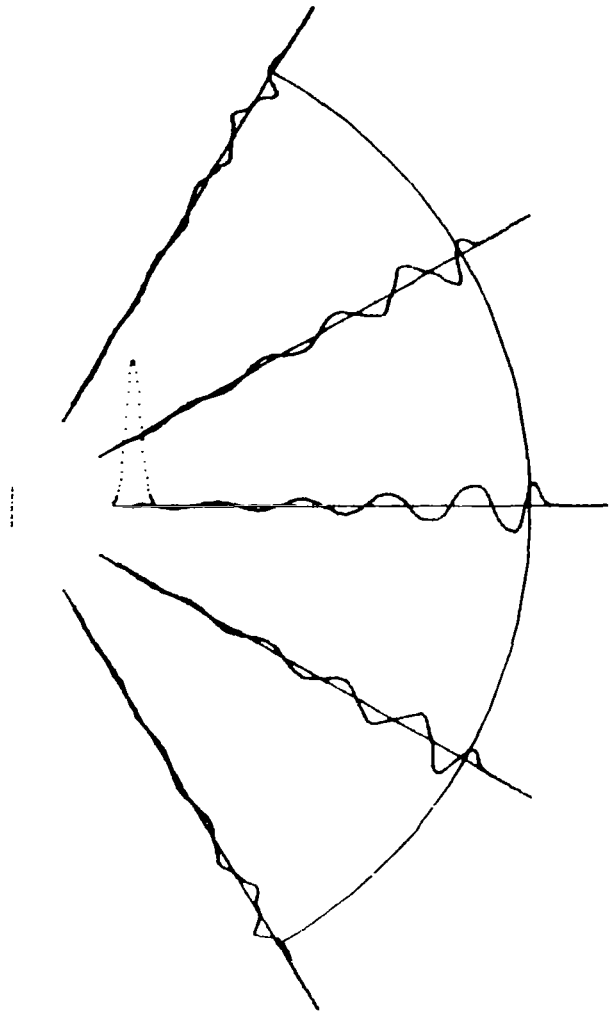

FIG. 19 Smoothed impulse response of finite wire with L/D=100 and θ^i 0^o .

As a final example, the result of scattering by a wire of length-to-diameter ratio of 100 with an oblique angle of incidence is displayed in Fig. 20. In this case the amplitude of the scattered field is smaller than for the case of normal incidence shown in Fig. 19; however, the rate of decay and period of the response remains essentially the same. Moreover, this provides an additional check on WSCAT in that it produces results which are consistent with the time-domain reciprocity theorem.[10] That is, the field scattered at -60° when the direction of incidence is 0° in Fig. 19 is the same as the field scattered at 0° when the direction of incidence is -60° in Fig. 20.

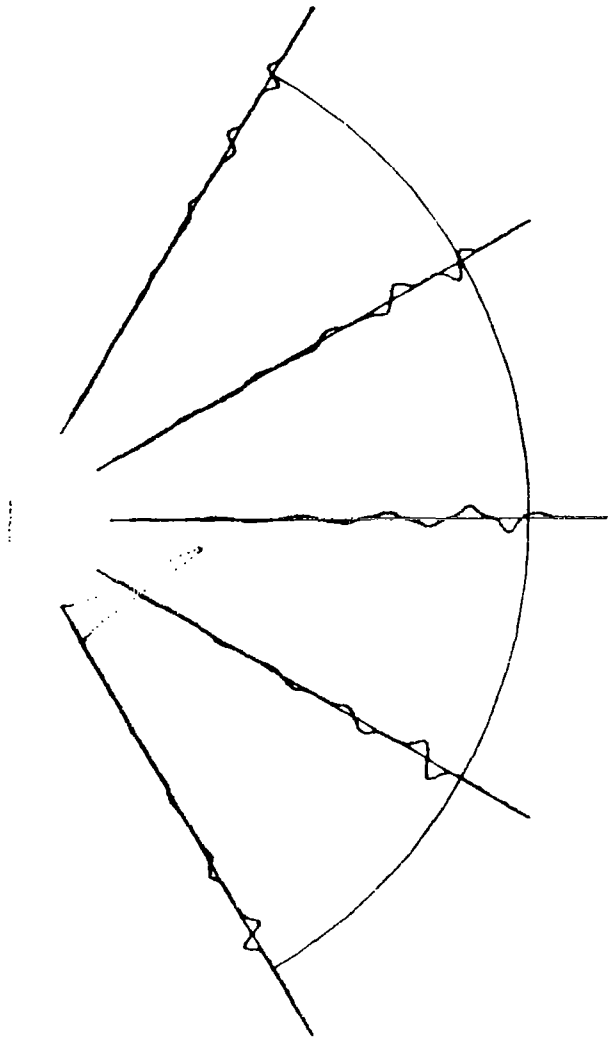

FIG. 20 Smoothed impulse response of finite wire with $L/D=100$ and $\theta^i=-60^\circ$.

SECTION 4

SCATTERING BY THREE-DIMENSIONAL CONDUCTING SURFACES WITH WIRES

The problem of determining the scattering by three-dimensional surfaces with wires attached is of great practical interest, since this serves as a model for numerous satellite-type objects that possess transmit and/or receive antennas. Moreover, to ignore the effect of the wire antennas will produce very poor results. To the authors' knowledge, there has been no adequate procedure developed for the solution of this complex scattering problem in either the time domain or the frequency domain. The following sections describe a new procedure that has been developed for solving this difficult scattering problem. Briefly, this procedure consists of the development of two simultaneous space-time integro-differential equations and their subsequent solution by marching on in time on a high-speed digital computer. These equations contain terms which may be interpreted as

(a) The influence of wire currents on other wire currents
(b) The influence of wire currents on surface currents
(c) The influence of surface currents on other surface currents
(d) The influence of surface currents on wire currents.

The neighborhood of the point where the wire is attached to the surface is accounted for by application of boundary conditions at the end of the wire.

4.1 DERIVATION OF SPACE-TIME INTEGRO-DIFFERENTIAL EQUATION

The technique used here to develop the space-time integro-differential equation for surfaces with wires is to consider the equivalent of this scattering problem shown in Fig. 21. In this equivalent statement of the problem the conducting surface has been replaced by source surface currents and the conducting wires have been replaced by source wire currents. Since these source currents are now radiating in free space, the techniques used for the case of scattering from surfaces alone can be combined with the technique used for the case of scattering from wires alone to solve the problem of scattering from surfaces with wires attached.

In particular, the space-time integral equation for surface currents that appears in Eq. (5) may be augmented by the magnetic field $\vec{H}_w(\vec{r},t)$ that

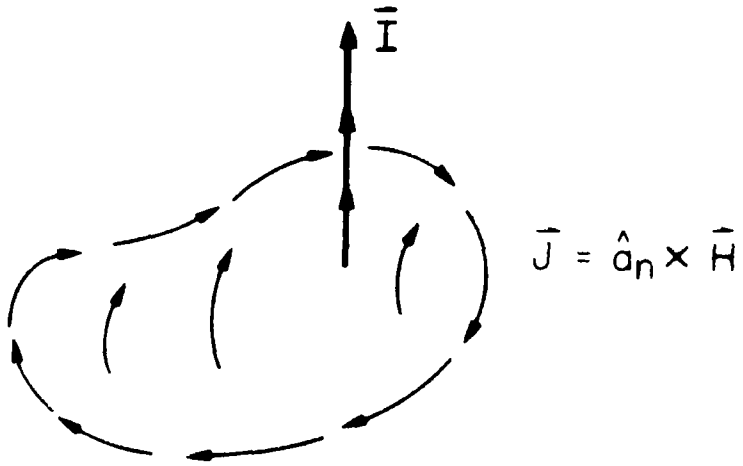

FIG. 21 Equivalent problem of scattering from surfaces with wires.

is produced by the wire currents, yielding the integral equation

$$\vec{J}(\vec{r},t) = 2\hat{a}_n \times \vec{H}^i(\vec{r},t) + 2\hat{a}_n \times \vec{H}_w(\vec{r},t)$$
$$+ \frac{1}{2\pi} \int_S \hat{a}_n \times \left\{ \left[\frac{1}{R^2} + \frac{1}{R} \frac{\partial}{\partial \tau} \right] \vec{J}(\vec{r}',t) \times \hat{a}_R \right\} dS' \qquad (31)$$
$$\tau = t - R$$

where the geometry parameters are defined in Sec. 2.2. The magnetic field $H_w(r,t)$ is found by applying the thin wire approximation to Eq. (1) to obtain

$$\vec{H}_w(\vec{r},t) = \frac{1}{4\pi} \int_\ell \left\{ \left[\frac{1}{R^2} + \frac{1}{R} \frac{\partial}{\partial t} \right] \vec{I}(\vec{r}',\tau) \times \hat{a}_R \right\} d\ell' \quad . \qquad (32)$$
$$\tau = t - R$$

The space-time integro-differential equation for the wire current that appears in Eq. (27) may be augmented by the electric field $\vec{E}_s(\vec{r},t)$ that is generated by the surface currents, producing the integro-differential equation

$$-\Omega I(x,t) = -\frac{1}{\alpha} \left[\sqrt{\frac{\epsilon}{\mu}} \frac{\partial E_x^i(x,t)}{\partial t} + \sqrt{\frac{\epsilon}{\mu}} \frac{\partial E_{sx}(x,t)}{\partial t} \right.$$
$$\left. + \frac{1}{4\pi} \Omega^2 \int_{\text{nonself}} \left\{ \frac{I(x',\tau)}{R} \right\} dx' \right] \qquad (33)$$
$$\tau = t - R$$

where the geometry parameters are defined in Sec. 3.1. At this point the wire is assumed to be parallel to the x-axis for ease of presentation. In this case it is necessary to compute only the x component of $\vec{E}_s(\vec{r},t)$. This is carried out starting with Maxwell's equation

$$\sqrt{\frac{\epsilon}{\mu}} \frac{\partial \vec{E}_s(\vec{r},t)}{\partial t} = \nabla \times \vec{H}_s(\vec{r},t) \qquad (34)$$

and the expression for $\vec{H}_s$,

$$\vec{H}_s(\vec{r},t) = \frac{1}{4\pi}\int_S \left\{\left[\frac{1}{R^2}+\frac{1}{R}\frac{\partial}{\partial\tau}\right]\vec{J}(\vec{r}',\tau)\times\hat{a}_R\right\}\,dS' \qquad (35)$$
$$\tau = t - R$$

where the units of time are light-meters.

Next, Eq. (35) is substituted into Eq. (34) and the indicated vector operations are carried out to give the x component of $\vec{E}_s(\vec{r},t)$ as

$$\frac{\epsilon}{\mu}\frac{\partial E_{sx}(\vec{r},t)}{\partial t} = \frac{1}{4\pi}\int_S \left[\frac{x-x'}{R^3}\left\{(x-x')\left[\frac{3}{R^2}+\frac{3}{R}\frac{\partial}{\partial\tau}+\frac{\partial^2}{\partial\tau^2}\right]J_x(\vec{r}',\tau)\right.\right.$$
$$+ (y-y')\left[\frac{3}{R^2}+\frac{3}{R}\frac{\partial}{\partial\tau}+\frac{\partial^2}{\partial\tau^2}\right]J_y(\vec{r}',\tau)$$
$$\left.+ (z-z')\left[\frac{3}{R^2}+\frac{3}{R}\frac{\partial}{\partial\tau}+\frac{\partial^2}{\partial\tau^2}\right]J_z(\vec{r}',\tau)\right\}$$
$$\left.- \frac{1}{R}\left\{\left[\frac{1}{R^2}+\frac{1}{R}\frac{\partial}{\partial\tau}+\frac{\partial^2}{\partial\tau^2}\right]J_x(\vec{r}',\tau)\right\}\right] dS' \qquad (36)$$
$$\tau = t - R$$

Thus, two simultaneous space-time integro-differential equations which are given in Eqs. (31) and (33) have been derived for the currents that are set up on a surface with attached wires.

It is of interest to examine the terms that appear in these two equations. Equation (31) gives the surface current in terms of the incident field, the wire currents, and other surface surrents. The first term is the source term and represents the influence of the incident field on the surface current. The second term on the right-hand side is the magnetic field produced by the wire currents and represents the influence of the wire currents on the surface currents. The third term on the right-hand side of Eq. (31) represents

the influence of the surface currents at other points on the surface current at the observer.

Equation (33) gives the wire current in terms of the incident field, the surface current, and other wire currents. The first term in the right-hand side is the source term, which is a function of the incident field. The second term is a function of the electric field produced by the surface currents and represents the influence of the surface currents on the wire currents. Finally, the third term on the right-hand side of Eq. (33) represents the influence of other wire currents on the wire current at the observer.

The wire currents at the free-space end and at the surface are given by the boundary conditions

$$\begin{aligned} I(x,t) &= 0 \qquad \text{free-space end} \\ \frac{\partial I(x,t)}{\partial x} &= 0 \qquad \text{surface end} \quad . \end{aligned} \tag{37}$$

Thus, the space-time integral equations (31) and (33) together with the boundary conditions in Eq. (37) and the defining relations in Eqs. (32) and (36) form the solution of the problem of scattering by surfaces with wires attached.

4.2 NUMERICAL SOLUTION

The numerical solution of Eq. (31) for the surface current was carried out in exactly the same manner as was the numerical solution of Eq. (5) and is described in detail in Sec. 2.3.1. The new feature in Eq. (5) is the addition of the term $2\hat{a}_n \times \vec{H}_w(\vec{r},t)$, which may be written as

$$2\hat{a}_n \times \vec{H}_w(\vec{r},\tau) + \left\{ \hat{a}_x \left[(y-y')n_y + (z-z')n_z \right] - \hat{a}_y \left[(y-y')n_x \right] - \hat{a}_z \left[(z-z')n_x \right] \right\} \left[\frac{1}{2\pi} \int_{\ell} \left\{ \frac{1}{R^3} + \frac{1}{R^2} \frac{\partial}{\partial \tau} \right\} I(x',\tau) \, dx' \right]_{\tau = t - R} . \tag{38}$$

The integration, differentiation, and interpolation in Eq. (38) were carried out numerically employing the techniques described in Sec. 2.3.3.

The numerical solution of Eq. (33) for the wire current was performed in exactly the same way as the solution of Eq. (27) and is described in detail in Sec. 3.2. The new feature in Eq. (33) is the addition of the electric field produced by the surface currents. This contribution was evaluated numerically from Eq. (36) using the techniques described in Sec. 2.3.3. Finally, the wire currents at the end of the wires were computed by numerical application of the boundary conditions in Eq. (37).

4.3 REPRESENTATIVE COMPUTATIONS

The computer program CSCAT was written to implement the procedures described in the previous section and used to solve the problem of scattering by conducting surfaces with wires attached. A program description and listing of CSCAT are presented in Vol. II. This program was checked out for the case of a finite wire on a ground plane and the result was in good agreement with the result obtained for the case of the finite wire in free space. The results obtained for two satellite models that have wires attached are now presented.

In Fig. 22 the small scientific satellite (SSS) model is shown. This consists of a sphere centered at the origin with four wire antennas protruding from the sphere along the positive and negative x and y axes. For the purpose of demonstrating the validity of the procedures that were presented in Sec. 4.2, the case of a vertically polarized incident wave on the SSS was considered, and the planar symmetry present was exploited.

Figure 23 displays the smoothed impulse response of SSS model that was computed by CSCAT. As noted previously, all dimensions in this "space snapshot" are drawn to scale except the distance from the target to the observer in the far field. At the center of this space snapshot is the contour of the SSS model, which is also drawn to scale. This figure displays the field scattered by this target in all directions. In particular, it is interesting to relate the response in the backscatter direction to the target geometry. The specular return from the nose of the sphere appears first and is of the same value as was obtained in Fig. 5 for the case of scattering by a sphere. Next, there is a second peak that can be attributed mainly to the specular return from the wire antennas. This is then followed by a damped oscillation

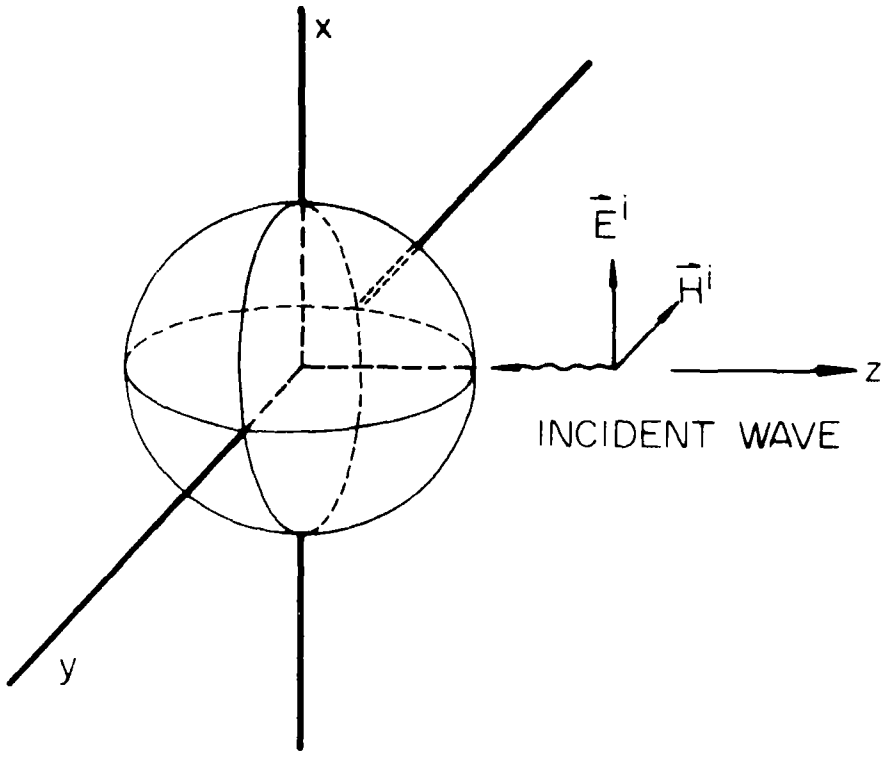

FIG. 22 SSS satellite model (length-to-diameter ratio of each antenna is 50).

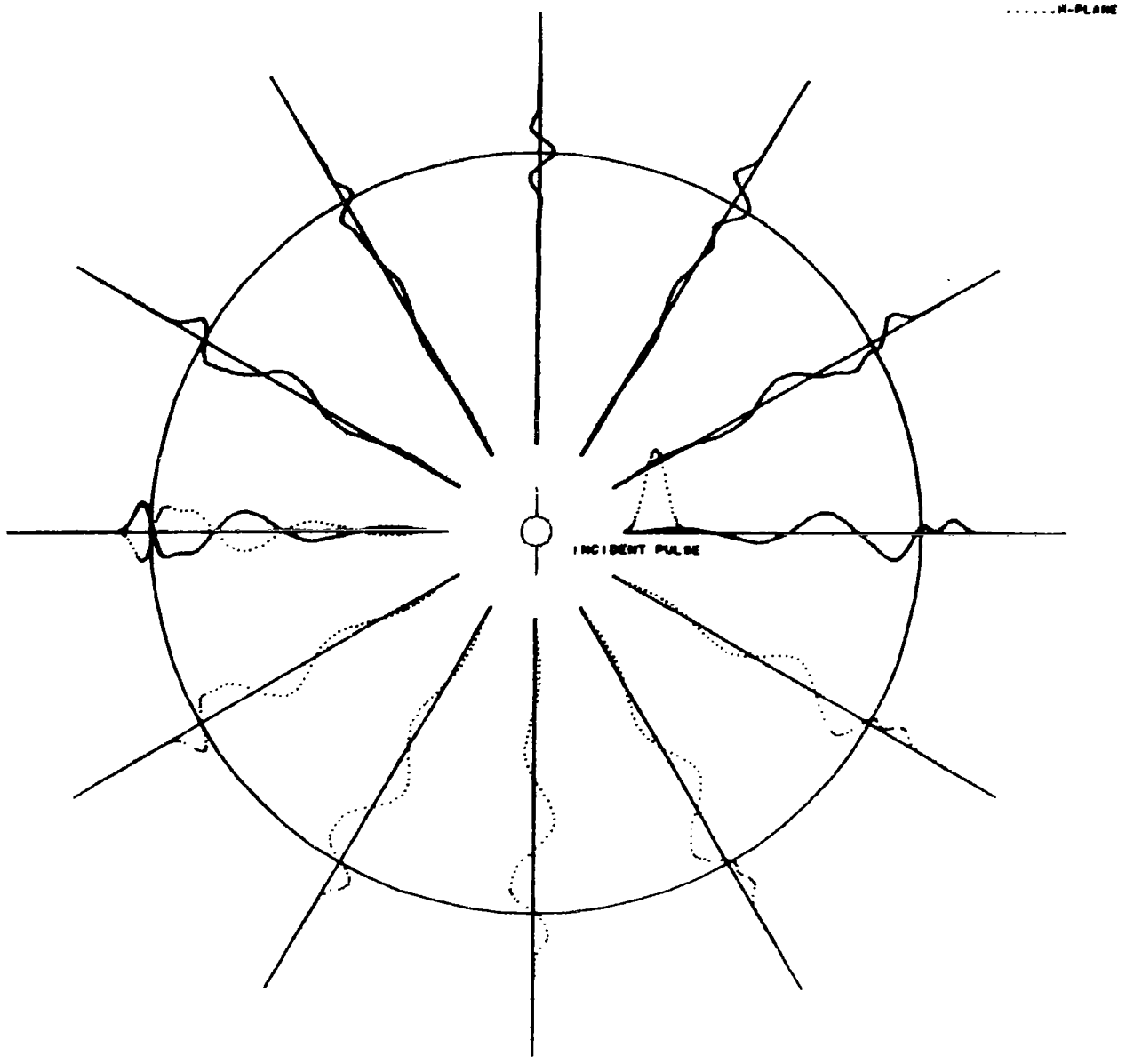

FIG. 23 Smoothed impulse response of SSS satellite model computed with CSCAT.

with a spacing between zero crossings that is approximately 2.5 sphere diameters. This is less than the distance between the opposite free tips of the wire (3 sphere diameters) but more than the length of an image representation of each antenna (2 sphere diameters). Moreover, the decay of these oscillations is much more rapid than would occur for the wires alone in free space with the same length-to-diameter ratio. This demonstrates the significant interaction between the antennas and the sphere surface.

As a check on the validity of these results a SSS model was fabricated and its smoothed impulse response was measured on the time-domain scattering range.[3] The result of this measurement was compared with the calculated SSS response. As can be seen in Fig. 24 the agreement is good.

The final satellite-type scatterer to be considered is the early warning reconnaissance satellite (EWRS). The model of this satellite is shown in Fig. 25. This model consists of a right circular cylinder with a length three times as large as the diameter. In addition, the cylinder has two antennas attached, each with a length equal to the cylinder diameter.

The smoothed impulse response of this target is shown in Fig. 26, along with the contour of the target. The initial portion of the response in the backscatter direction approximates the derivative of the incident pulse and can be attributed to the front end of the cylinder. This is followed by a damped oscillation that may be attributed mainly to the currents traveling on the wires. After the third positive peak in the backscatter response, a departure from regularity in the damped oscillation can be noted. The timing of this departure indicates that it is due to a return from the back edge of the cylinder.

Finally, as a check on the validity of these calculated results, a model of the EWRS was fabricated and the smoothed impulse response was measured in the backscatter direction. The result of this measurement is compared in Fig. 27 with the calculated response and demonstrates the good agreement that was obtained.

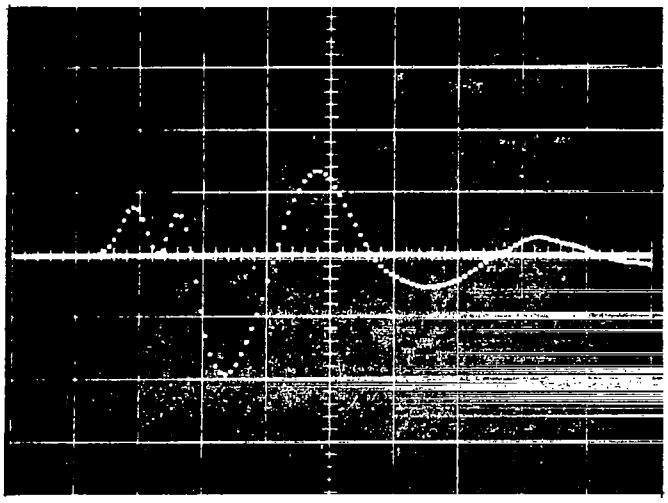

(a) Measured SSS response
(horiz. scale = 0.5 nsec/div.)

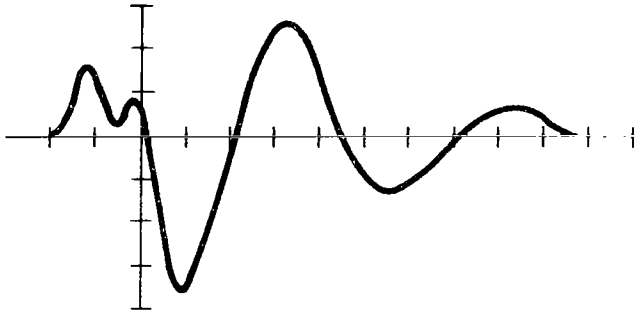

(b) Calculated SSS response

FIG. 24 Comparison of calculated and measured SSS response in backscatter direction.

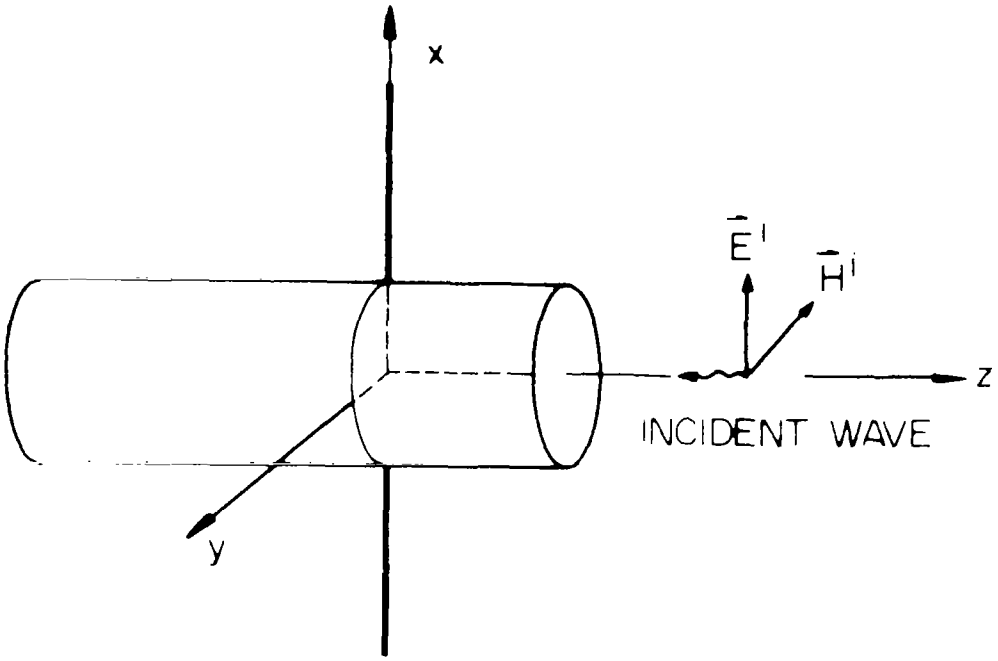

FIG. 25 EWRS satellite model (length-to-diameter ratio of each antenna is 50).

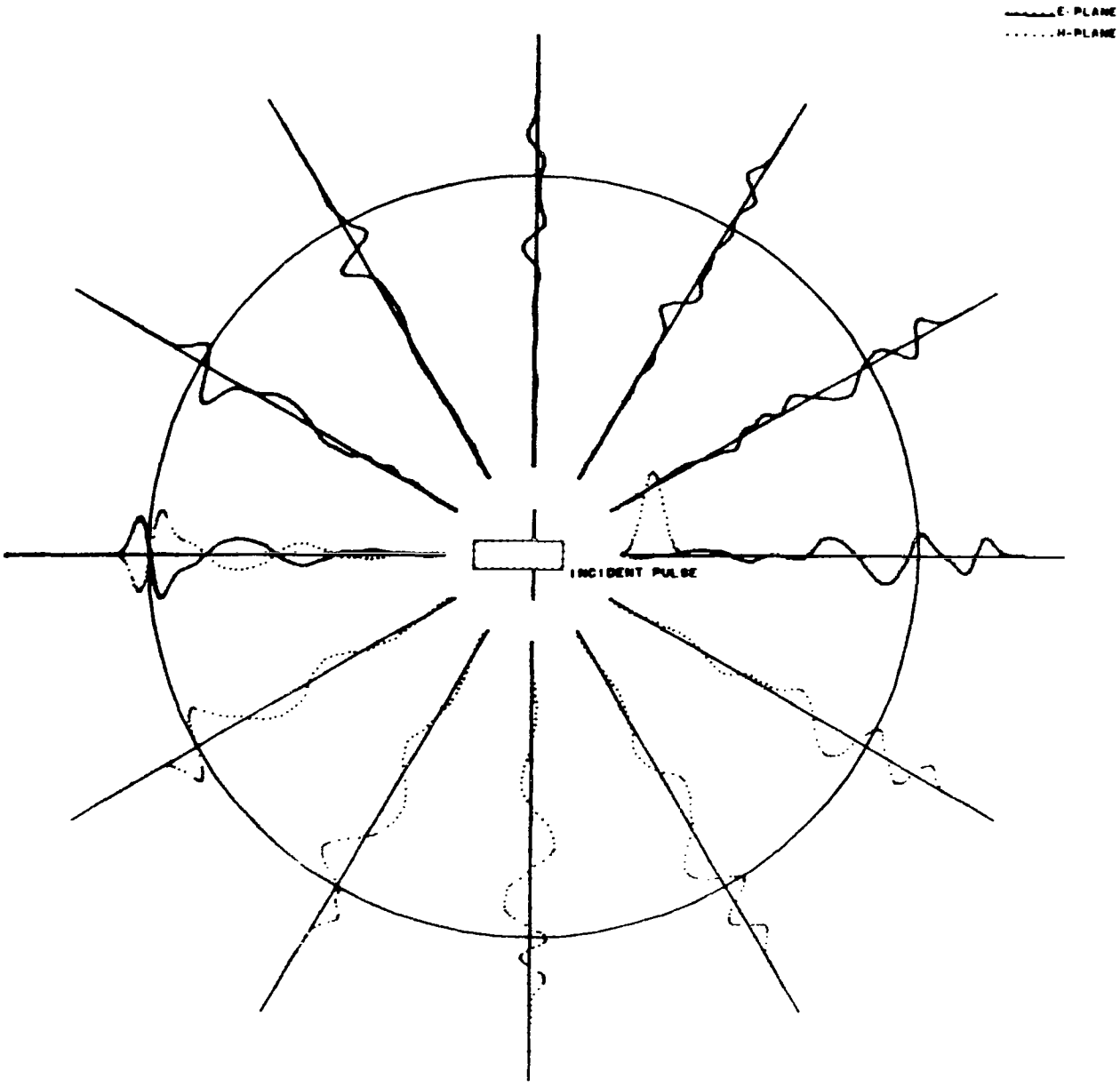

FIG. 26 Smoothed impulse response of EWRS satellite model computed with CSCAT.

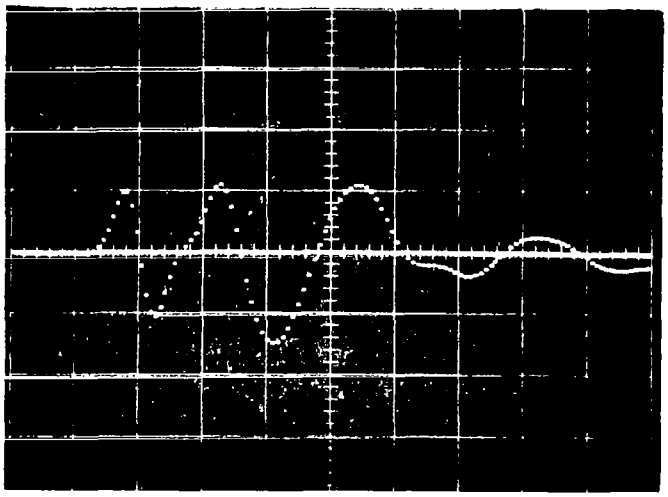

(a) Measured EWRS response
(horiz.scale = 0.5 nsec / div.)

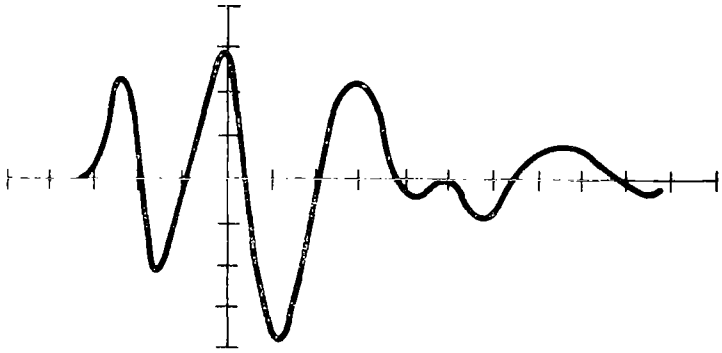

(b) Calculated EWRS response

FIG. 27 Comparison of calculated and measured EWRS response in backscatter direction.

SECTION 5

CONCLUSIONS

The results of this study demonstrate that the space-time integral equation approach to short-pulse scattering calculation is extremely powerful. Moreover, these solutions are carried out directly in the time domain in much the same manner that nature herself solves the problem in the real world, eliminating the time-consuming process of matrix inversion that in the past has been used to solve the integral equation in the frequency domain.

In particular, procedures have been developed and implemented for five cases of the general scattering problem. These specific cases are:

(1) asymmetric scattering problems involving composite surfaces,

(2) plane symmetric scattering problems involving composite surfaces,

(3) rotationally symmetric scattering problems involving composite surfaces,

(4) scattering by finite wires, and

(5) scattering by surfaces with wires attached.

In this work new and significant techniques have been developed for the solution of the problem of scattering by finite wires and the solution of the problem of scattering by surfaces with wires attached. These procedures have then been applied to satellite-type objects which include the UES, ADC, GGTS-2, SSS, and EWRS satellites, and the smoothed impulse responses of these targets were computed. Finally, it is important to note that the calculated responses have been compared with measured responses from the time-domain scattering range and that the agreement was good.

The technique at present is limited by the size of the body relative to a pulse width that may be treated practically. The procedures developed here give good results for body sizes up to several pulse widths. Treatment of larger bodies at this time is restricted by limitations of high-speed computer memory and running times.

The next logical phase in the solution of short-pulse scattering problems is the extension of the space-time integral equation approach to bodies which are much larger than a pulse width.

SECTION 6

REFERENCES

1. C. L. Bennett, W. L. Weeks, "A Technique for Computing Approximate Electromagnetic Impulse Response of Conducting Bodies," Interaction Note 222, June 1968.

2. J. D. DeLorenzo, "Electromagnetic Transient Studies in Space Time," Ph.D. Thesis, Boston University, Boston, Mass., May 1970.

3. C. L. Bennett and J. D. DeLorenzo, "Short Pulse Response of Radar Targets," 1969 International Antenna and Propagation Symposium, Austin, Texas, December 1969.

4. J. H. Richmond, "Digital Computer Solutions of Rigorous Equations for Scattering Problems," Proc. IEEE 53, 796 (1965).

5. R. L. Tanner and M. G. Andreason, "Numerical Solution of Electromagnetic Problems," IEEE Spectrum 4, 53 (1967).

6. R. F. Harrington, Field Computation by Moment Methods (The Macmillan Company, New York), 1968.

7. E. P. Sayre, "Transient Response of Wire Antennas and Scatterers," Ph.D. Thesis, Syracuse University, Syracuse, New York, June 1969.

8. E. P. Sayre and R. F. Harrington, "Transient Response of Straight Wire Scatterers and Antennas," 1968 International Antenna and Propagation Symposium, Boston, Mass., September 1968.

9. R. Courant, K. Friedrichs and H. Lewy, "Über die partiellen Differenzengleichungen der mathematischen Physik," Mathematische Annallen 100, 32 (1928).

10. B. R. Cheo, "A Reciprocity Theorem for Electromagnetic Fields with General Time Dependence," IEEE Trans. AP-13, 278-284 (1965).